Theses, Dissertations and Culminating Projects

5-2014

Late Pliocene Ice-Rafted Debris Mass Accumulation Rates from IODP Site U1359, Wilkes Land Continental Rise, Antarctica

Jessica Rosenberg
Montclair State University

Recommended Citation

MONTCLAIR STATE UNIVERSITY

Late Pliocene Ice-Rafted Debris Mass Accumulation Rates from IODP Site U1359,

Wilkes Land Continental Rise, Antarctica

By

Jessica Rosenberg

A Master's Thesis Submitted to the Faculty of

Montclair State University

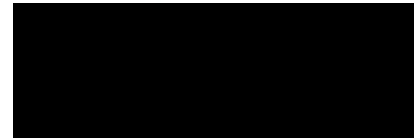In Partial Fulfillment of the Requirements
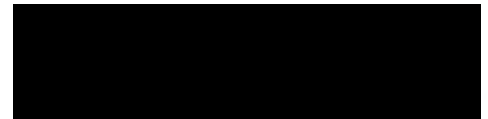
For the Degree of

Master of Science

May 2014

College/School College of Science and Mathematics
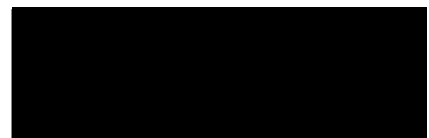
Department Earth & Environmental Studies

Thesis Committee:

Dr. Sandra Passchier
Thesis Sponsor

Dr. Stefanie A. Brachfeld
Committee Member

Dr. Gregory Pope
Committee Member

Abstract

An assessment of sediments taken from the IODP (Integrated Ocean Drilling Program) Expedition 318, Core U1359A from the Wilkes Continental Land Rise, has been conducted at a high resolution to determine the response of the East Antarctic Ice Sheet to climate during the Late Pliocene. The section of core being studied dates back to ~3.7 to 2.7 million years ago (Ma). Studies can lead to an understanding of climate change in the future, from knowledge on how ice sheets have transformed in the past with similar atmospheric conditions to the present. Samples from this record were analyzed based on the bulk particle size distributions, which were determined using a Malvern Mastersizer 2000 laser diffractometer. The samples were treated to remove organics, opal, and biogenic carbonate. The data was then processed using the coarse fraction, grater than 125 microns to calculate ice rafted debris (IRD) mass accumulation rates (MAR). After analysis of IRD, an additional analysis of microtextures using a scanning electron microscope (SEM) was conducted on high peaks of IRD. This test confirmed that sediments were glacially derived. By comparing the IRD MAR record to temperature, sea level, CO_2 levels, $\partial^{18}O$ records, and seismic data, it was determined that peaks in IRD MAR coincide with an expanding ice sheet. The IRD record from Hole U1359A between 3.7 and 2.7 Ma reflects an IRD signal of ice sheet advance, with matching peaks and trends in other proxies.

LATE PLIOCENE ICE-RAFTED DEBRIS MASS ACCUMULATION RATES FROM

IODP SITE U1359, WILKES LAND CONTINENTAL RISE, ANTARCTICA

A THESIS

Submitted in partial fulfillment of the requirements

for the degree of Masters of Science

by

JESSICA ROSENBERG

Montclair State University

Montclair, NJ

2014

Table of Contents   **Page**

List of Figures   **Page**

List of Tables   **Page**

Chapter 1: Introduction

Understanding the dynamics of the Antarctic Ice Sheet is important for past, present and future studies of Earth's climate. It is known that the cryosphere plays an important role in ocean circulation, sea level and temperature. Studies can be conducted on how the climate will change in the future, from knowledge on how ice sheets have transformed in the past with similar atmospheric conditions to the present. The Pliocene closely represents the 21st century in terms of a similar CO_2, and thusly it is very important to study this period of time in geologic history (Murphy et al., 2002).

About 3.3 to 3.0 million years ago was the last time mean surface temperatures on Earth were warmer than present for a long period of time (Masson-Delmotte et al., 2013). This warm period is known as the Mid-Pliocene Warm Period, characterized by a ~20 m or higher rise in sea level above present (Miller et al., 2012). Carbon dioxide concentrations during the Pliocene were also similar to today, but most likely higher than preindustrial values (Fedorov et al., 2013). In fact, Pliocene CO_2 levels were between 350 and 450ppm (Masson-Delmotte et al., 2013), as compared to the current CO_2 concentration from January 2014, of 397 ppm (NOAA/ESRL, 2013). Understanding the climate distribution and forcing for the Pliocene period may help improve predictions of the likely response to a change in CO_2 in the future, including the ultimate role of the ocean circulation in a globally warmer world. It is just as important to understand a cooling climate as well. The Pliocene is known for a long-term increase of sea ice globally, and a decrease in temperature from ~3.3 to 2.6 Ma (Masson-Delmotte et al., 2013).

This study focuses on the Late Pliocene, where CO_2 levels begin to drop and

transition into the Pleistocene, a glacially driven climate. Knowledge of this transition period may provide the basis for future climate predictions.

1.1 Site Location and Background: IODP Expedition 318

Integrated Ocean Drilling Program (IODP) Expedition 318 was carried out in 2010. This study examines U1359 Hole A from the Wilkes Land Continental Rise in Antarctica (Figure 1). The Wilkes Land margin terminates at the seaward side of the East Antarctic subglacial basin, and is located below sea level (Escutia et al., 2005). This would indicate that the site is more susceptible to change; i.e. sea level, temperature, and ocean circulation. The continental shelf is up to 125 km wide with a water depth of ~440-500 m; a loading of ice and sediments along with glacial erosion causes an over deepening and a slope landward in bathymetric profile (Escutia et al., 2005). Escutia et al. (2005) describe the topography of the shelf as irregular with deep basins on the inside of the shelf, troughs that become more shallow as they navigate from the inner to the more shallow outer shelf banks. In some places, greater than 1000 meter deep inner-shelf basins occur at the mouths of the outlet glaciers. The glaciers are an important mechanism in the delivery of sediment into the ocean.

During a tectonic episode separating Antarctica and Australia, in the mid-Jurassic/Cretaceous, the Wilkes Land continental margin is said to have formed (Escutia et al., 2005). Site U1359 is located at 3009 meters below sea level (mbsl) on the continental rise on the eastern levee of the Jussieau submarine channel, where the relief is ~400 m (Expedition 318 Scientists, 2010).

Hole A was drilled to a total depth of 193.50 meters below sea floor (mbsf) with an

80% recovery (Expedition 318 Scientists, 2010). The dominant lithology throughout the core is silty clay with dispersed clasts, variable amounts of biogenic components, and bioturbation with dispersed sets of silt-sand laminae, and variable amounts of biogenic silica and calcite abundances. Three lithostratigraphic units were observed in four drill holes [U1359A-D] including Unit II which lies between 43.5 and 247.1 mbsf, consisting of bioturbated silty clays containing diatoms, interbedded with diatom-bearing silty clays that are olive-gray in color with decimeter packages of olive-brown silty clay with silt laminae within them. The sedimentology represents levee deposition by turbidity currents, most likely low in density. The diatom-bearing silty clays represent a high productivity environment, and a time of minimal ice cover.

1.2 Objectives

There are many uncertainties regarding the climate of the Pliocene in the Antarctic. With an increase in CO_2 comes an increase in global temperatures, potentially affecting the size of polar ice sheets. Considering CO_2 affects on the ice sheet in the Pliocene, will further the understanding of ice sheet response to increasing CO_2 levels in the future. Carbon dioxide levels during the late Pliocene (~3.4- 2.4 Ma) show a decrease, which coincides with an escalation in global ice volume (Fedorov et al., 2013). This decrease in CO_2 may indicate a cooling trend, which could potentially be found in a record of ice rafted debris (IRD).

IRD represents material that has been entrained within an iceberg that has calved from a marine based ice sheet or glacier, and has been transported to its ultimate destination. Surface waters are cold enough to not melt the iceberg before it reaches its

destination. Deposition of IRD comparative to warm or cold cycles in climate is important in understanding how icebergs carrying IRD are produced (Williams et al., 2010). Changes within a margin of ice will produce icebergs and eventually deposit debris to the seabed. Iceberg calving rates are also related to ice discharge into the ocean. Thus, higher discharge rates of the glacier would increase delivery of IRD.

Sediment cores can give an uninterrupted and long time frame for studying climate change. For understanding the local climate drivers in Antarctica during the Pliocene with higher CO_2 levels, as compared to today, a record of ice rafting can be constructed. During the Late Pliocene, however, there is evidence to suggest a slight decrease in CO_2 levels in the atmosphere from records compiled by Seki et al. (2010). Ice-rafted detritus mass accumulation rates (IRD MAR) are interpreted to indicate the extent of the ice sheet during the Late Pliocene. High levels of IRD MAR would indicate advancement of ice, whereas low levels of IRD MAR indicate that the surface waters may have been too warm for the iceberg to reach the site, or no icebergs were being produced. Higher flow rates of a glacier would indicate ice growth, and increased calving rates (Passchier, 2011). This would increase delivery of IRD. IRD MAR maxima can be associated with an expanding ice sheet, as well as a retreating one. Both scenarios could produce icebergs that would ultimately deposit IRD to the sea floor. Multiple studies have been conducted on this site, and others (Murphy et al., 2002, Passchier, 2011, Williams et al., 2010) on the East Antarctic Ice Sheet (EAIS), none of which have been as high of a resolution as those in this study. Looking at temperature, sea level change, CO_2 levels, $\partial^{18}O$ records, and seismic data, it can be determined whether the peaks in IRD coincide with glacials or interglacial.

Chapter 2: Methods

2.1 Laser Particle Sizer Sample Preparation

A high-resolution particle size analysis has been completed for Hole U1359A, for ~ 48 to 70 mbsf using a Malvern Mastersizer 2000 laser particle sizer. The instrument located at Montclair State University is outfitted with a Hydro 2000MU pump. Approximately 150 samples were taken from this section at ~13 cm intervals to analyze the terrigenous particle size. The samples were pretreated first to remove any calcareous and siliceous biogenic compounds.

The pre-treatment process followed Konert and Vandenberghe (1997), Appendix C. Thirty percent hydrogen peroxide and 10% hydrochloric acid were used to remove the organic material that was incorporated in the sediments (Konert and Vandenberghe, 1997). The clay size fraction has a high surface-to-volume ratio, which would increase the attractive forces between particles (Sperazza et al., 2004). With clay particles stuck together, this would cause the particle sizer to read the clay as one larger grain rather than many small grains, thus skewing the results. Sodium pyrophosphate was used as a dispersing agent for the samples in this project.

To achieve an accurate measurement of grain size, the appropriate amount of sediment must be used, thus receiving a satisfactory range for obscurations, which is between 10 and 20% for fine-grained sediment (Sperazza et al., 2004). If too much or too little sample is used, the obscurations become too high or low, respectively. Approximately 100 mg of each sample was broken off from each section. The sample was then placed into a 250 mL beaker. Ten mL of hydrogen peroxide was then poured

into the beaker and slightly stirred to mix the hydrogen peroxide into the sample. The beaker was then transferred onto a hot plate under a fume hood. As soon as a reaction began, millipore water was poured into the beaker to have the solution reach 25 mL. The same millipore water was used throughout the entire process. The sides of the beaker were washed with the water as well to assure that any particles that may have spattered on the sides would reenter suspension. When reactions ceased, 5 mL of 10% hydrochloric acid and water were added to the beaker to bring the solution up to 50 mL. The mixture was then brought back up to a boil for 10 to 15 minutes or until the reaction stopped. The beaker was then removed from the hotplate to cool. Once the solution in the beaker was cool, the sample was transferred to a 50 mL polypropylene centrifuge tube, and using more distilled water to rinse all material into the tube to fill it to 50 mL. The sample was then placed into a centrifuge to rotate at 1800 rpm for 30 minutes, then the supernatant was decanted, and the tube was refilled with more water. The tubes were shaken and replaced into the centrifuge for 30 minutes at 1800 rpm. The supernatant was then removed for a second time.

The tube was then filled with 5 mL of sodium hydroxide, to remove the biogenic silica, with a concentration of 1 N, and ~20 mL of water to fill the tube with 25 mL of solution. The tubes were then placed into a hot bath at 87° Celsius for one hour. After the hour, they were taken out to cool before they were then filled with an additional 25 mL of water and placed back into the centrifuge for 30 minutes at 1800 rpm. The supernatant was then decanted. The samples were then rinsed out of the tubes into the original 250 mL beakers, and filled to 50 mL with water. A small amount of the dispersant, sodium pyrophosphate ($Na_4 P_2O_7 \cdot 10H_2O$), was added to each beaker, and

returned to the hotplate. Samples were barely boiled, to make sure the dispersant was completely dissolved before they were removed and left under the fume hood to cool.

The Malvern Mastersizer 2000 laser diffractometer software was opened, and the laser was turned on to warm up. Two 850 mL beakers containing the millipore water were prepped, and one was placed into the Hydro 2000MU sample dispersion unit. Another 850 mL beaker was prepped for the sample and was filled with water that had been sitting to allow air bubbles to escape. The pump was then turned on, and the water pumped through the instrument to remove any previous sample, and clean out the tubes. Once the background became stable, the beaker was removed, and the beaker with millipore water that had been sitting out was placed into the Hydro2000 MU unit, and measured for background. The pump propeller unit was then lifted up, a sample was then added, and the beaker and placed into the pump, and the rotor was turned on. Water may have then been added to achieve the desired obscuration, and measurements were started. If optimal obscuration was not reached, or if the obscuration was too high, the sample number was noted to be rerun at a later date. After measurements were saved to the computer, the sample was poured into a waste container, and the beaker was cleaned, and filled with water for the next sample to be run. Two 850 mL beakers of water were then run through the instrument to ensure that all sediment from the previous sample was removed, before the next sample was to be run. This process was implemented for each sample.

2.2 Instrumentation

The Malvern Mastersizer 2000 laser diffractometer with Hydro 2000MU pump accessory uses two light sources, a red He-Ne laser at 0.632 μm, and a blue LED at

0.466 μm to diffract light off the surface of the particles (Sperazza et al., 2004). The

standard operating procedure implemented was based on the method by Sperazza et al.

(2004); separating coarse-grained peaks from fine-grained peaks using bulk particle size

analysis. It is complicated to determine the primary refractive index (RI) of natural

sediments because the sediment is a mix of minerals with different indices of refraction

(Sperazza et al., 2004). Sperazza et al. (2004) determined the RI by the sum of the

product of the different refractive indices and the percent volume abundance for each

mineral, using X-ray diffraction (Sperazza et al., 2004). For this study, the coarser

grains are quartz, and the fine fraction is illite (Shipboard Scientific Party, 2001). The

RI for illite was used because it was most abundant. Thus, the marine sediment

standard operating procedures, associated with Montclair State University's laser

particle sizer, were implemented. Determining the degree of absorption of sediments

that are natural is difficult because the parameter changes with grain shape, particle

size, chemical alteration of grains, coatings on the grains, and the extend of abrasion on

the surface (Sperazza et al., 2004). Absorption ranges from 0 to 1, perfectly clear to

perfectly opaque (respectively) (Sperazza et al., 2004). Because the sediments were

assumed to be mostly illite grains, the RI is 1.54 and the absorption index is 0.9, also in

Montclair State University's marine sediment standard operating procedures.

Diffracted light is measured by 52 sensors and accumulated in 100 size fraction

bins (Sperazza et al., 2004). The turbulence created by the pump propeller suspends the

sediment, and keeps it suspended throughout the measurement (Sperazza et al., 2004).

The speed of the pump was determined by the range indicated in Sperazza et al., (2004),

and the size of grains in the samples. The range recommended is 1800-2300 rpm, and

the speed used was 2200 rpm, which kept the particles suspended in solution, giving optimal obscuration results.

The best obscuration results can be achieved by introducing an ideal amount of sediment. This amount of sediment will be enough to accurately depict the overall size of the grains in the entire sample, but not enough to be impenetrable by the laser (Sperazza et al., 2004). Sperazza et al. (2004) recommends the range of obscuration to be 15 to 20% for fine-grained lake sediments, however, considering the wide range of particle sizes present in the samples from Hole U1359A, the obscuration range used for this project was between ~10 and 35%.

With samples having too high or too low of an obscuration value, 14 samples had to be re-run to achieve accurate results. With collection of the acceptable obscurations, a comparison was made to the original high or low obscuration with the optimal result to determine the difference it makes. Graphs were generated for each sample comparing the original obscuration (high or low) versus the ideal obscuration value that had been re-run.

2.3 IRD MAR Calculations

The data collected from the particle sizer was used to calculate the ice rafted debris (IRD) mass accumulation rate (MAR) using the equation:

$$IRD\ MAR = IRD \times TERR \times DBD \times LSR$$

Where IRD % is the measured volume percent of grains greater than 125 microns, TERR is the terrigenous fraction according to the methodology of Krissek

(1995), calculated as 100-biogenic silica (Song et al., 2012). DBD is the dry bulk density, which is derived from shipboard measurements (Shipboard Scientific Party, 2011). The LSR is the linear sedimentation rate (cm/y), which is calculated from the age model.

The age model (Figure 2) is based on magnetic tie points, which are correlated with depth from Tauxe et al. (2012) in Table 1. Two linear regression lines were fit to create two different linear sedimentation rates, shown in Figures 3 and 4, one for ~44 to 68 mbsf, and another for ~68 to 69 mbsf. With these rates, IRD MAR can be calculated accordingly.

2.4 Scanning Electron Microscope Method

A total of 3 samples were taken, one from each peak in IRD MAR in Figure 5. These samples were analyzed using a scanning electron microscope (SEM) to determine the origin and transport modes of the grains. By completing this further analysis, it can be determined that the peaks in IRD MAR are consistent with IRD and not another process of deposition.

The samples were suspended and wet sieved using millipore water and 63-micron mesh to clean off the larger quartz grains from any clay particles that may be stuck to them. Once most of the clay was cleared away, the quartz grains were then transferred into a dish to dry in an oven at 75 degrees celsius. After the grains were visibly dry and all water was evaporated away, the dish was taken to be viewed under a light microscope. Using thin tweezers, the quartz grains were carefully transferred to an aluminum stub using double-sided carbon tape. Approximately 35 to 40 random quartz

grains were taken from each sample and placed on a stub. The stubs were then coated with gold using the Denton Desk IV TSC Cold Sputter/Etch and then put into the SEM for analysis.

The grains were analyzed using a Hitachi S-3400N SEM with an accelerating voltage of 12 kV, as used by Strand et al. (2003). The composition of each grain was also examined using a Bruker X-Flash energy dispersive x-ray spectrometer to confirm the quartz mineralogy of the grains. An SEM image was collected of each grain, using the Secondary Electron Detector, on every stud for further analysis. Once scans were made of all of the grains, the scans were then analyzed using a classification scale by Damiani et al. (2006). The grains used for the Damiani et al. (2006) classification are marine sediments from the Pleistocene- Quaternary, from Wilkes Land Continental Rise, which is the same location of the grains in this study, thus this classification scale is ideal for use in this record. Grain Type 1 is characterized by sharp edges and high relief with numerous conchoidal fractures and very few or no forms of chemical alteration, and is indicative of a glacial origin (Damiani et al., 2006). An example of a Type 1 grain with conchoidal fractures can be seen in Figure 22. Type 2 grains, also glacial in origin, contain the same features as Type 1, but are sub-angular to sub-rounded with medium to low relief and smoothed edges. Solution pits and silica pellicles may be observed on some surfaces. An example of grain Type 2 can be seen in Figure 23. Type 3 grains are classified as sub-angular to sub-rounded with medium to low relief, with the same microfeatures as Type 2, but with high chemical alteration partially obliterating their surfaces. They contain a thick coat of amorphous silica, and are indicative of glacial-subaqueous grains. These features can be seen in Figure 26.

Type 4 grains are sub-rounded to rounded with smoothed edges and low relief, with irregular depressions of different sizes. They have evidence of chemical solution pits, and precipitation of silica, and are characterized as grains from a marine environment, such as subaqueous transport from bottom currents. An example of grain Type 4 can be seen in Figure 30. Type 5 grains are highly rounded, and show an abundance of upturned plates, and dish shaped concavities on the surface, seen in Figure 31. They are indicative of an eolian origin. Type 6 grains, have highly modified surfaces due to chemical activity, with a predominance of silica precipitation features, and are representative of grains which sat in a high-chemical diagenetic setting. An example of grain Type 6 can be seen in Figure 32.

Chapter 3: Results

3.1 Particle Size Distribution

The predominant terrigenous sediment type for Hole U1359A from ~47 to 70 mbsf is silt based on the particle size analysis, with volume percentages ranging from 48 to 80 as shown in Figure 6. Spanning downward in the section, the volume percent of silt generally shows an increasing trend, though there are many fluctuations. The next highest volume percent range is clay spanning from 12 to 49 percent. Again, fluctuations are present, but the general trend in the section is decreasing from 47 to 70 mbsf. Sand is the least dominant sediment type, which ranges from 0 to 30 percent by volume.

3.2 Obscuration Results

During the first set of samples being run through the particle sizer, a total of 14 samples were beyond the limit of optimal obscuration. A new batch of these 14 samples was prepared and put back through the particle sizer to achieve an acceptable obscuration value, and thus more accurate results. Figures 7-20 compare the results from the two different runs. The original run (Run 1) resulted in either too high or too low of an obscuration to be able to use. The redo-run (Run 2) contained obscurations within the ideal range.

Run 1 shown in Figures 7, 9, 10, and 12 represent obscurations that were higher than 40%. Figures 7, 9 and 12 all exhibit similar obscurations when comparing Run 1 and Run 2, even though Run 1 contained obscuration values considered to be too high to be accurate. However, it is apparent in Figure 9 that having more sediment in suspension caused the distribution to favor larger grain sizes, skewing the peak towards the right, and flattening it out. Figures 8, 13, 14, 15, 16, 17, 18, 19, and 20 all compare an obscuration considered too low to be accurate. For all 9 figures, the first peak is generally the same for both runs, however in Figures 14, 16, and 20, in Run 1, a second peak emerges around 1000-1414 μm, whereas in Run 2, there is no second peak. In Figures 8, 13, 15, 17, and 18, no significant change between Run 1 and Run 2 is noted. In Figure 19, Run 2 exhibits a second peak at 1414 μm. Run 1 in Figure 11 demonstrates a dissimilar pattern of peaks.

3.3 IRD MAR Results

IRD MAR generally decreases with depth and age in U1359A, shown in Figure 5. Large peaks of IRD MAR can be seen at 2.87 Ma, 3.13 Ma and 3.32 Ma. Generally, these high peaks coincide with low levels of silt and clay. Because of the closed sum problem, this is to be expected.

3.4 Microtexture Results

Once peaks in IRD MAR are recognized, it is important to verify that the peaks are from ice rafting. Using the SEM will help in determining the origin of the grains from the three peaks, shown in Figure 5 by the red arrows.

Forty-two grains (Table 1) were analyzed using the SEM for the first peak at ~2.9 Ma. Using the classification scale by Damiani et al. (2006), 16% of the grains are Grain Type 1, 26% are Type 2, 38% are Type 3, 4% are Type 5, and 14% are Type 6 (Chart 1). Thirty-four grains are glacial in origin, 2 are eolian, and 6 are diagenetic (Table 4). Figure 22, Figure 23, and Figure 24 are all examples of Grain Type 1, Grain Type 2, and Grain Type 3 (respectively) taken from this peak in IRD MAR (U1359A 7H 4W).

Forty-two grains (Table 2) were analyzed for the second peak at ~3.1 Ma. 0% of the grains are Grain Type 1, 14% are Type 2, 62% are Type 3, 2% are Type 4, 5% are Type 5, and 17% are Type 6 (Chart 2). Thirty-three grains are glacial in origin, 1 is marine, 2 are eolian, and 7 are diagenetically altered (Table 5). Figure 25, and Figure 26 are all examples of Grain Type 2 and Grain Type 3 (respectively) taken from this peak in IRD (U1359A 8H 4W). Figure 30 is an image of the marine grain found in this

sample. Figure 31 is an example of an eolian grain from this sample. Figure 32 is an example of a chemically altered grain from this sample.

Thirty-nine grains were analyzed for U1359 sample 9H 1W (Table 3). 7% are Grain Type 1, 36% are Type 2, 49% are Type 3, and 8% are Type 6 (Chart 3). Thirty-six grains are glacial in origin and 3 grains are diagenetically altered (Table 6). Figure 27, Figure 28, and Figure 29 are all examples of Grain Type 1, Grain Type 2, and Grain Type 3 (respectively) taken from this peak in IRD (U1359A 9H 1W).

Chapter 4: Discussion

4.1 Obscuration Analysis

After analyzing the figures (7-20) and comparing Run 1 to Run 2 in all re-run samples, it seems to be clear that adding more sediment or taking away sediment from the samples makes little difference. Though optimal obscurations are between 15 and 20%, it is observed that having too much sediment or too little sediment compared to the ideal amount recommended made little to no change. If too much sample was added to the solution, for example in Figure 7, it might be expected to see a peak around 1000 μm, if there were to be a difference at all. However, though the obscuration in Run 1 is 43.49%, there is very little difference between Run 1 and Run 2, which has an optimal obscuration of 23.61%. Another example is if too little sediment is used, resulting in an obscuration that is too low (according to the recommended amount). In Figure 14 with Run 1 of 2.77% and Run 2 of 14.64%, it would be expected that there would be no peak around 1000 μm because there would be too few grains to pick up a large grain in the graph. However, a peak is noted in Run 1 at ~1414 μm whereas, that peak is not found

in Run 2 (which has optimal obscuration). A possible explanation for this could be that air bubbles became trapped in the water, and thus were run through the instrument, and read as a grain. However, overall this conclusion identifies that though optimal obscuration is between 15 and 20%, and in this study was extended to 10 and 35%; there is no noted pattern between having too little sample, or too much sample with a second peak. The general trend of the graphs between the two runs is almost identical.

4.2 Microtexture Analysis

By analyzing microtextures from grains in 3 peaks of the IRD record from U1359A (Figure 5), it has been determined that most grains are glacially derived. Eighty-one percent of the grains in the first sample, taken from 7H 4W, are glacially derived. Seventy-six percent of the grains in 8H 4W are glacially derived. Sixty-two percent of the grains in 8H 4W are type 3, or modified glacial grains. This peak in IRD MAR (at ~62.1 mbsf) lines up with a sequence of fining upward clay in the lithostratigraphy. This correlation can be seen in Figure 40. This may indicate that the grains were originally glacial, and then finally deposited by a low density turbidity current. Ninety-two percent of the grains taken from 9H 1W are glacially derived. With these results, it can be concluded that turbidity currents, wind processes, or any other process did not deposit the majority of the grains. The grains from U1359A from ~3.7 to 2.7 Ma were deposited from a glacier, or iceberg.

4.3 IRD Analysis and Ice Sheet Dynamics

Studying IRD is important in understanding the dynamics of an ice sheet during a particular period in time. Based on the IRD MAR record from core U1359A from ~3.7 to 2.7 Ma, IRD MAR increases up-core, thus indicating the increase in movement of icebergs over the core site as time passes. Because IRD MAR is limited to tracking the intensity of ice rafting over the site, not whether it was advancing or retreating, other proxies must be interpreted to fully understand how IRD is being formed, whether the ice sheet advanced or retreated.

According to McKay et al. (2012), a cooling trend within the coastal seas of Antarctica can be seen in sedimentary facies, sea surface temperature reconstructions, and diatom assemblages. It is reported that the West Antarctic Ice Sheet had expanded into the Ross Sea during the Late Pliocene and Early Pleistocene (McKay et al., 2012). The Ross Sea, shown in Figure 1, is west of the Wilkes Land Rise. This confirmed decrease in temperature can be seen in the IRD MAR record of U1359, as an increasing trend in IRD. According to Miller et al. (2012) an increase in sea level of ~22 m above present level, from 3.2 to 2.7 Ma indicates a loss of ice from Greenland and the WAIS, with some volume loss from the EAIS. With the data used by Miller et al. (2012), taken from the United States, New Zealand, and the north Pacific Ocean, an expected ~10 m sea level contribution from the EAIS is expected. As an observation, in Figure 2 from Miller et al. (2012) a slight decreasing trend can be seen in sea level from 3.3 to 2.7 Ma. In the record of IRD MAR from U1359A, from 3.2 to 2.7 Ma, there is a slight increase. Decreasing sea level, and temperature, and increasing IRD suggests that there is an

increase in ice volume occurring. To further confirm the ice sheet dynamics, CO_2 levels must also be examined.

It is known that the Late Pliocene is indicative of a transition from a warm time period with CO_2 levels reaching over 400 ppm (Pagani et al., 2010) to a cooler Pleistocene, with lower CO_2 levels. Comparing a CO_2 record by Seki et al., (2010), with the IRD record from U1359 (Figure 31), the general trend of CO_2 decreases up-core. Levels of ~400 ppm exist at 3.7 Ma, with a gradual decrease to ~350 at 3.3 Ma. At 3 Ma, a large peak of CO_2 reaches ~415 ppm before a decrease from 3 Ma to 2.7 Ma. Though there is an oscillation of CO_2, the decreasing trend confirms Pagiani et al. (2010), and further verifies the CO_2 levels within the section of time in which this study is occuring. The uncertanties for the different approaches used by Seki et al. (2010) provide a high level of confidence in the accuracy of the record. Whitehead et al. (2005) reports that marine sediment was deposited inland, which would confirm a retreat of ice. This reduction in sea ice occurred at ~3.1 Ma, at Sites 1165 and 1166 (both located in Prydz Bay shown in Figure 1). The only option for the ice to retreat to the extent being reported is for CO_2 levels to be twice those of pre-industrial values (Raymo et al., 1996 and Whitehead et al, 2005). This is very unlikely, so it is thought that minor changes in the atmosphere must be considered to be the cause. Figure 34 shows the CO_2 levels during this time period according to Seki et al. (2010). The peak noted previously at ~3 Ma could possibly account for this retreat, especially if minor changes in the atmosphere are to be considered. It is possible that Sites 1165 and 1166 were affected by this change and U1359 was not.

The $\partial^{18}O$ record will aid in determining exactly what the ice was doing at a particular period in time because it provides information on ice volumes. This will give further insight into whether there was more or less ice at the Wilkes Land Rise from 3.7 to 2.7 Ma. O^{18} Levels are a useful proxy because having more O^{18}, the heavier isotope, would mean that more O^{16} is being held up in glacial ice because it is lighter. Thus, high levels of O^{18} indicate more glacial ice, and low levels would indicate less glacial ice. Figure 21 shows the IRD MAR record alongside the $\partial^{18}O$ record. A general increasing trend can be seen in both graphs.

Figure 33 is a compilation of the $\partial^{18}O$ record alongside the IRD MAR record for U1359A with magnetostratigraphy. There are two noted periods where the $\partial^{18}O$ record seems to be elevated for an extended period of time. The first period is from ~3.42- 3.27 Ma, occurring across the boundary of the C2An.3n Chron and the following reversal. This is known as the M2 glacial, which begins just at ~3.35 Ma (Lisiecki and Raymo, 2005). This glacial advance can be seen across Antarctica, in other records as well (Passchier, 2011). The next noted similarities in IRD MAR and the benthic record is not a period of time, but a single peak. This peak occurs in the C2An.2n Chron, at ~ 3.17 Ma. This would most likely indicate a brief surge of ice. This peak can be compared to a peak from the record in Murphy et al. (2002), seen in the same chron. The last period of time that indicates ice expansion is ~3.05- 2.7 Ma in the C2An.1n Chron. These ice-advance records are highlighted in blue. The later two peaks also coincide with peaks of IRD seen in Passchier (2011). This would indicate that the event can be seen throughout Antarctica.

To further confirm this expansion, seismic records can be compared as well. Based on seismic profiles collected by the international Wilkes Basin Glacial History Project, interpreted by De Santis et al. (2003) and Escutia et al. (2005), the seismic sequence WL-S9 occurred during the Pliocene-Pleistocene (as confirmed by Escutia et al., 2011). This can be seen in figure 38. This sequence is interpreted as forming under full polar conditions due to the noted decrease in sediment supply; when most of the sediment that was being deposited on the margin, ended up being trapped on the outer shelf and slope creating prograding wedges (Escutia et al., 2005 and De Santis et al., 2003), which is confirmed by Escutia et al. (2011). Site U1358, located on the outer continental shelf of Wilkes Land, can be seen in Figure 39. The record for Site U1358 contains intervals of no deposition between 3.99 Ma to 0.61/0.54 Ma (Orejola and Passchier et al., 2013). Because there is limited age control for the drill-hole, no correlation in seismic data can occur, however, with the hiatus within the time period in this study, it can be inferred that there was glacial advance due to the lack of sediment being deposited.

Chapter 5: Conclusion

Having detailed knowledge of a record of IRD MAR during the Pliocene can be extremely helpful in interpreting data for future climate predictions. Because ice plays such an important role in ocean circulation, sea level and temperature, this detailed information is significant to understanding how the current and future climate is influenced.

Using the Malvern Mastersizer 2000 laser diffractometer to conduct a grain size analysis gave way to a study in optimal obscurations. Though the recommended obscuration results should be from 15 to 20% (Sperazza et al., 2004), it was found that extremely low obscurations, and extremely high obscurations yielded similar results. Little to no change was found between the low or high run compared to the run characterized as optimal.

After IRD MAR were calculated using the coarse fraction of the particle size data, and three peaks of relatively large quantities of IRD MAR were noted. A microtextural analysis was conducted using an SEM to determine the origin of the IRD, whether it is glacial, eolian, marine, or too chemically altered to decipher. The results concluded that all three peaks contain a large majority of glacially derived grains. With knowledge that the record is predominantly glacial, this makes it easier to compare to other proxies.

Temperature, sea level, and CO_2 records give an insight into what the climate was like during the Late Pliocene. With a cooling trend that can be seen in coastal seas of Antarctica, an observed general trend of decreasing sea levels, and an overall decrease in CO_2, an increase in ice volume can be confirmed. This increase can be seen in the overall trend of IRD MAR from U1359A between 3.7 and 2.7 Ma.

Benthic records indicate three intervals with elevated levels of $\partial^{18}O$ in foraminiferal carbonate. The first period of time is from ~3.42- 3.27 Ma, occurring at the boundary of the C2An.3n Chron and the following reversal. The second is a single peak that occurs in the C2An.2n Chron, at ~ 3.17 Ma. This would most likely indicate a brief surge of ice. The third increment that indicates ice expansion is ~3.05- 2.7 Ma in

the C2An.1n Chron. All three elevated intervals coincide with intervals of high levels in IRD MAR. This confirms that both the benthic $\partial^{18}O$ record and the IRD MAR record reflect simultaneous ice sheet advances and retreats. Seismic records are also in agreement with an ice sheet advance from 3.7 to 2.7 Ma. Comparing seismic data from the seismic sequence WL-S9, a decrease in sediment load was observed. This would indicate that the ice had advanced to the outer shelf, and beyond the location in which the data was extracted at IODP Site U1358. Temperature, CO_2, $\partial^{18}O$ levels, and seismic records all concur with the IRD MAR record during the Late Pliocene. The IRD MAR record from U1359A between 3.7 and 2.7 Ma reflects an IRD signal of ice sheet advance, with matching peaks and trends in other proxies. This knowledge helps give an understanding in how the ice sheet of the Late Pliocene reacted to changes in climate.

Bibliography

Damiani, D., Giorgetti, G., and Turbans, I. M., (2006). Clay mineral fluctuations and surface textural analysis of quartz grains in Pliocene–Quaternary marine sediments from Wilkes Land continental rise (East-Antarctica): Paleoenvironmental significance. *Marine Geology, 226,* (281-295).

De Santis, L., Brancolini, G., and Donda, F., (2003). Seismo-stratigraphic analysis of the Wilkes Land continental margin (East Antarctica): influence of glacially driven processes on the Cenozoic deposition. Deep-Sea Research. Part 2. *Topical Studies in Oceanography, 50* (8–9), (1563–1594).

Escutia, C., Brinkhuis, H., and Klaus, A., and the Expedition 318 Scientists, (2011). *Proceedings of the Integrated Ocean Drilling Program,* Volume 318. doi:10.2204/iodp.proc.318.101.2011

Escutia, C., De Santis, L., Donda, F., Dunbar, R.B., Cooper, A.K., Brancolini, G., (2005). Cenozoic ice sheet history from East Antarctic Wilkes Land continental margin sediments. *Global and Planetary Change, 45,* (51-81).

Expedition 318 Scientists, (2010). Wilkes Land Glacial History: Cenozoic East Antarctic Ice Sheet evolution from Wilkes Land margin sediments. *IODP Prel. Rept.,* 318.

Grützner, J., Hillenbrand, C-D., and Rebesco, M., (2005). Terrigenous flux and biogenic silica deposition at the Antarctic continental rise during the late Miocene to early Pliocene: implications for ice sheet stability and sea ice

coverage. *Global Planet Change, 45*, (131–149),

doi:10.1016/j.gloplacha.2004.09.004.

Jansen, E., Overpeck, J., Briffa, K.R., Duplessy, J.-C., Joos, F., Masson-Delmotte, V.

… and 43 others, (2007). Palaeoclimate. In: Climate Change 2007: The Physical

Science Basis. Contribution of Working Group I to the Fourth Assessment

Report of the Intergovernmental Panel on Climate Change. [Solomon, S., Qin,

D., Manning, M., Chen, Z., Marquis, M., Averyt, K.B., Tignor, M., and Miller,

H.L. (eds)]. Cambridge University Press, Cambridge, United Kingdom and New

York, NY, USA.

Konert, M., and Vandenberghe, J., (1997). Comparison of laser grain size analysis with

pipette and sieve analysis; a solution for the underestimation of the clay fraction.

Sedimentology, 44 (535).

Krissek, L., (1995). Late Cenozoic ice-rafting records from Leg 145 sites in the North

Pacific: Late Miocene onset, late Pliocene intensification, and Pliocene-

Pleistocene events. In *Proceedings of the Ocean Drilling Program. Scientific

results, 145*, (179-194). Ocean Drilling Program.

Lisiecki, L.E., and Raymo, M.E., (2005). A Pliocene–Pleistocene stack of 57 globally

distributed benthic δ18O records, *Paleoceanography*, 20.

Masson-Delmotte, V., Schultz, M., Abe-Ouchi, A., Beer, J., Ganopolski, J.F., González,

R., Jansen, E., Lambeck, K., Luterbacher, J., Naish, T., Osborn, T., Otto-

Bliesner, B., Quin, T., Ramesh, R., Rojas, M., Shao, X., Timmerman, A.,

(2013). Information from Paleoclimate Archives. In: *Climate change 2013: The Physical Science Basis. Contribution of Working Group I to the Fifth Assessment Report of the Intergovernmental Panel on Climate Change.* [Stocker, T.F., D. Qin, G.-K. Plattner, M. Tignor, S.K. Allen, J. Boschung, A. Nauels, Y. Xia, V. Bex and P.M. Midgley (eds.)]. Cambridge University Press. Cambridge, United Kingdom and New York, NY. USA.

McKay, R., Naish, T., Carter, L., Riesselman, C., Dunbar, R., Sjunneskog, C., Winter, D., Sangiorgi, F., Warren, C., Pagani, M., Schouten, Stefan., Willmott, V., Levy, R., DeConto, R., and Powel, R.D., (2012). Antarctic and Southern Ocean influences on Late Pliocene global cooling. *Earth, Atmospheric, and Planetary Sciences* (1-6) www.pnas.org/cgi/doi/10.1073/pnas.1112248109.

Miller, K. G., Wright, J. D., Browning, J. V., Kulpecz, A., Kominz, M., Naish, T. R., ... & Sosdian, S. (2012). High tide of the warm Pliocene: Implications of global sea level for Antarctic deglaciation. *Geology, 40*(5), 407-410.

Murphy, L., Warnke, D. A., Andersson C., Channell, J., and Stoner, J., (2002). History of ice rafting at South Atlantic ODP Site 177-1092 during the Gauss and late Gilbert Chrons. *Palaeogeography, Palaeoclimatolgy, Palaeoecology, 182*(3), (183-196).

National Oceanic Atmospheric Association/Earth System Research Laboratory, (2013). *Trends in Atmospheric Carbon Dioxide.* Retrieved from http://www.esrl.noaa.gov/gmd/ccgg/trends/mlo.html.

Orejola, N., Passchier, S., and Expedition 318 Scientists, (2013). Sedimentology of

> Lower Pliocene to Upper Pleistocene diamictons from IODP Site U1358,
>
> Wilkes Land margin, and implications for East Antarctic Ice Sheet Dynamics.
>
> *Antarctic Science.* (1-10). doi:10.1017/S0954102013000527

Pagani, M., Liu, Z., LaRiviere, J., and Ravelo, A., (2010). High Earth-system climate

> sensitivity determined from Pliocene carbon dioxide concentrations. *Nature*
>
> *Geoscience, 3*, (27-30).

Passchier, S., (2011). Linkages between East Antarctic Ice Sheet extent and Southern

> Ocean temperatures based on a Pliocene high-resolution record of ice-rafted
>
> debris off Prydz Bay, East Antarctica. *Paleoceanograhy, 26,* PA4204,
>
> doi:10.1029/2010PA002061.

Raymo, M.E., Grant, B., Horowitz, M., and Rau, G.H., (1996). Mid-Pliocene warmth:

> Stronger greenhouse and stronger conveyor: Marine Micropale- ontology, *27,*
>
> (313–326).

Rebesco, M., Camerlenghi, A., Geletti, R., and Canals, M., (2006). Margin architecture

> reveals the transition to the modern Antarctic ice sheet ca. 3 Ma, *Geology, 34*
>
> (4), 301-304, doi: 10.1130/G22000.1.

Ryan, W.B.F., S.M. Carbotte, J.O. Coplan, S. O'Hara, A. Melkonian, R. Arko, R.A.

> Weissel, V. Ferrini, A. Goodwillie, F. Nitsche, J. Bonczkowski, and R. Zemsky
>
> (2009), Global Multi-Resolution Topography synthesis, Geochem. Geophys.
>
> Geosyst., 10, Q03014, doi:10.1029/2008GC002332.

Seki, O., Foster, G.L., Schmidt, D.N., Mackensen, A., Kawamura, K., and Pancost,

R.D., (2010). Alkenone and boron-based Pliocene pCO_2 records. *Earth and*

Planetary Science Letters. (201-211). doi:10.1016/j.epsl.2010.01.037

Shipboard Scientific Party (2001). Site 1165, in: Ocean Drilling Program Initial Reports

188, edited by P.E. O'Brien, A.K. Cooper and C. Richter,

doi:10.2973/odp.proc.ir.188.103.2001.

Song, B., Khim, B.K., and Katsuki, K. (2012). *Variation of Biogenic Opal Content from*

Quaternary to Late Neogene on the Continental Rise of Wilkes Land (Sites

U1359 & U1361, IODP Exp 318), East Antarctica. Poster session presented at

the Scientific Committee on Antarctic Research (SCAR), Portland, Oregon.

Sperazza, M., Moore, J.N., and Hendrix, M.S., (2004). High-resolution particle size

analysis of naturally occurring very fine-grained sediment through laser

diffractometry. *Journal of Sedimentary Research, 74(5),* (736-743).

Strand, K., Passchier, S., and Näsi, J., (2003). Implications of quartz grain microtextures

for onset Eocene/Oligocene glaciation in Prydz Bay, ODP Site 1166, Antarctica.

Palaeogeography, Palaeoclimatology, Palaeoecology, 198(1), (101-111).

Tauxe, L., Stickley, C.E., Sugisaki, S., Bijl, P.K., Bohaty, S.M., Brinkhuis, H., Escutia,

C., Flores, J.A., Houben, A.J.P., Iwai, M., Jiménez-Espejo, F., McKay, R.,

Passchier, S., Pross, J., Riesselman, C.R., Röhl, U., Sangiorgi, F., Welsh, K.,

and 13 others, (2012). Chronostratigraphic framework for the IODP Expedition

318 cores from the Wilkes Land Margin: constraints for paleoceanographic reconstruction. *Paleoceanography, 27(2).*

Tripati, A.K., Roberts, C.D., Eagle, R.A., (2009). Coupling of CO_2 and Ice Sheet Stability Over Major Climate Transitions of the Last 20 Million Years. *Science, 326,* (1394-1397).

Williams, T., van de Flierdt, T., Hemming, S.R., Chung, E., Roy, M., and Goldstein, S.L., (2010). Evidence for iceberg armadas from East Antarctica in the Southern Ocean during the late Miocene and early Pliocene. *Earth and Planetary Science Letters, 290,* (351-361).

Whitehead, J.M., Wotherspoon, S., and Bohaty, S.M., (2005). Minimal Antarctic sea ice during the Pliocene. *Geology,* (137-140).

Figures
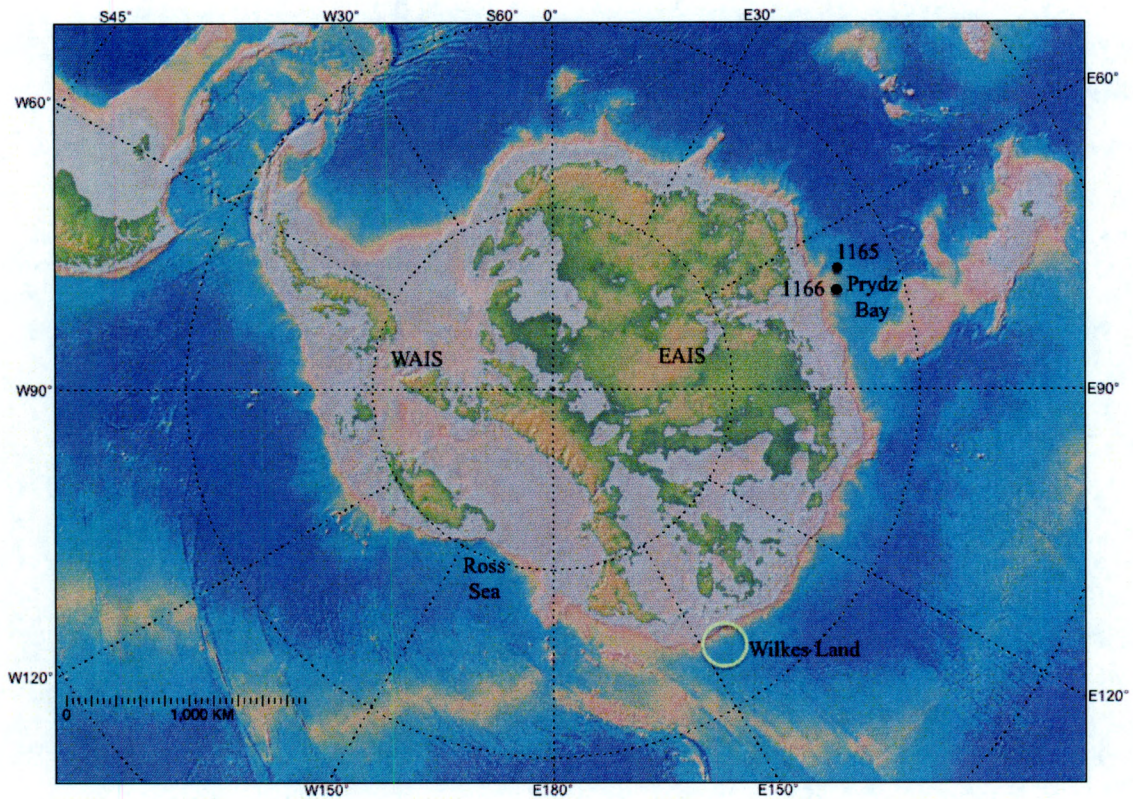
Figure 1. Site Location (circled), and location of the Ross Sea and Prydz Bay and locations of Sites 1165 and 1166. (http://www.geomapapp.org).
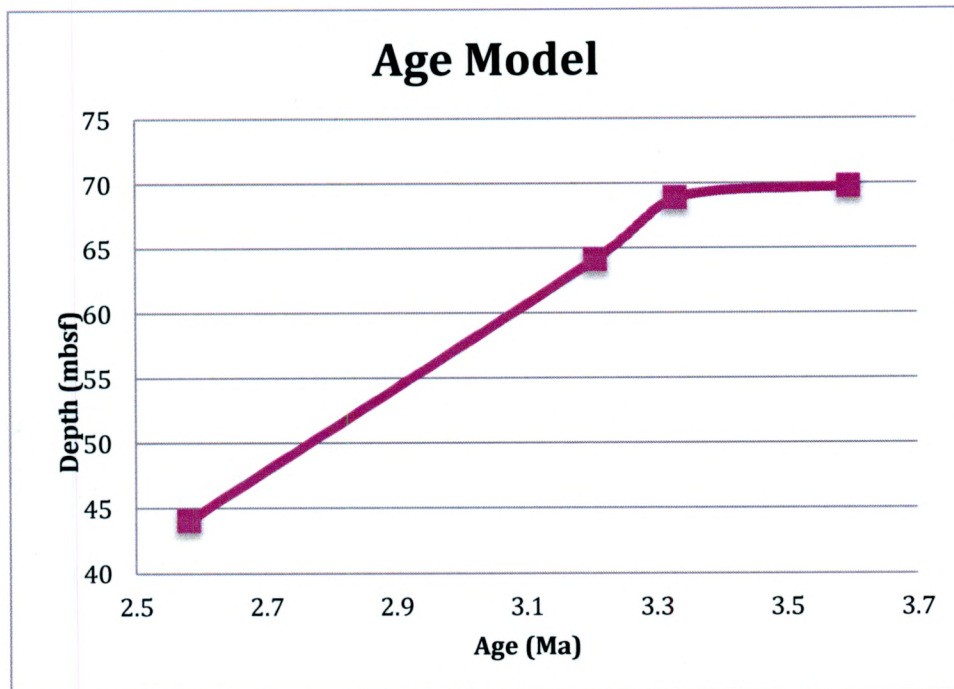
Figure 2. Age model for U1359A from ~44 to ~70 mbsf.
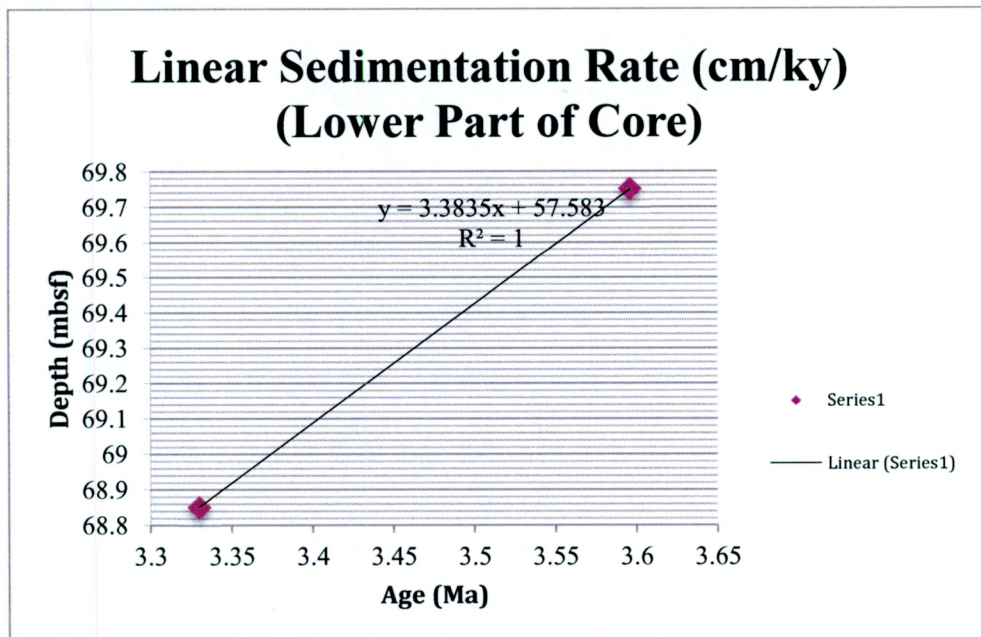
Figure 3. Linear sedimentation rate calculation for the lower part of the core (~68.8 to 69.8 mbsf).
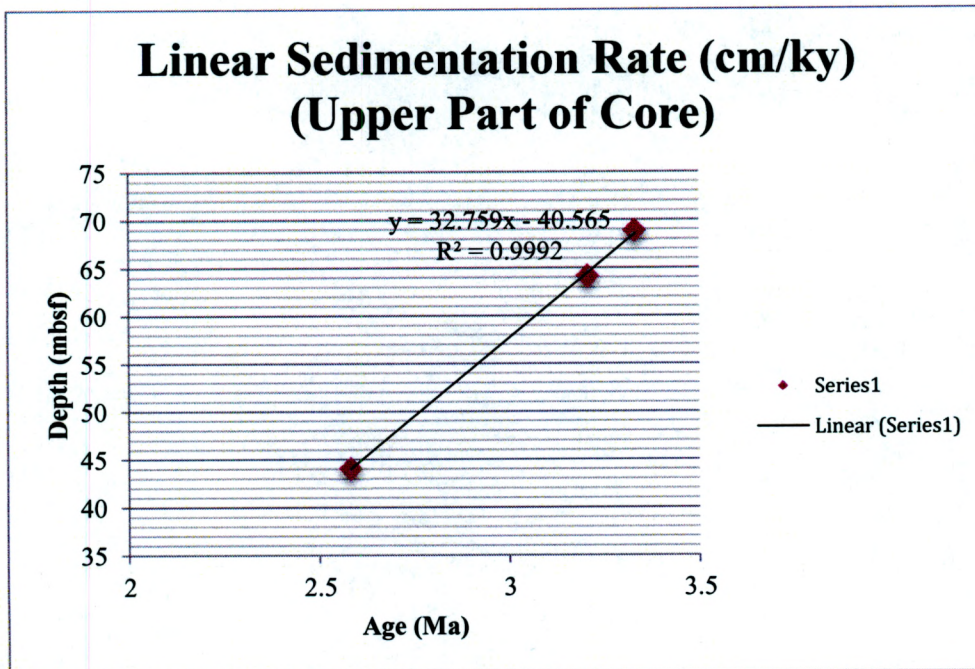
Figure 4. Linear sedimentation rate calculation for the upper part of the core (~44 to 68 mbsf).
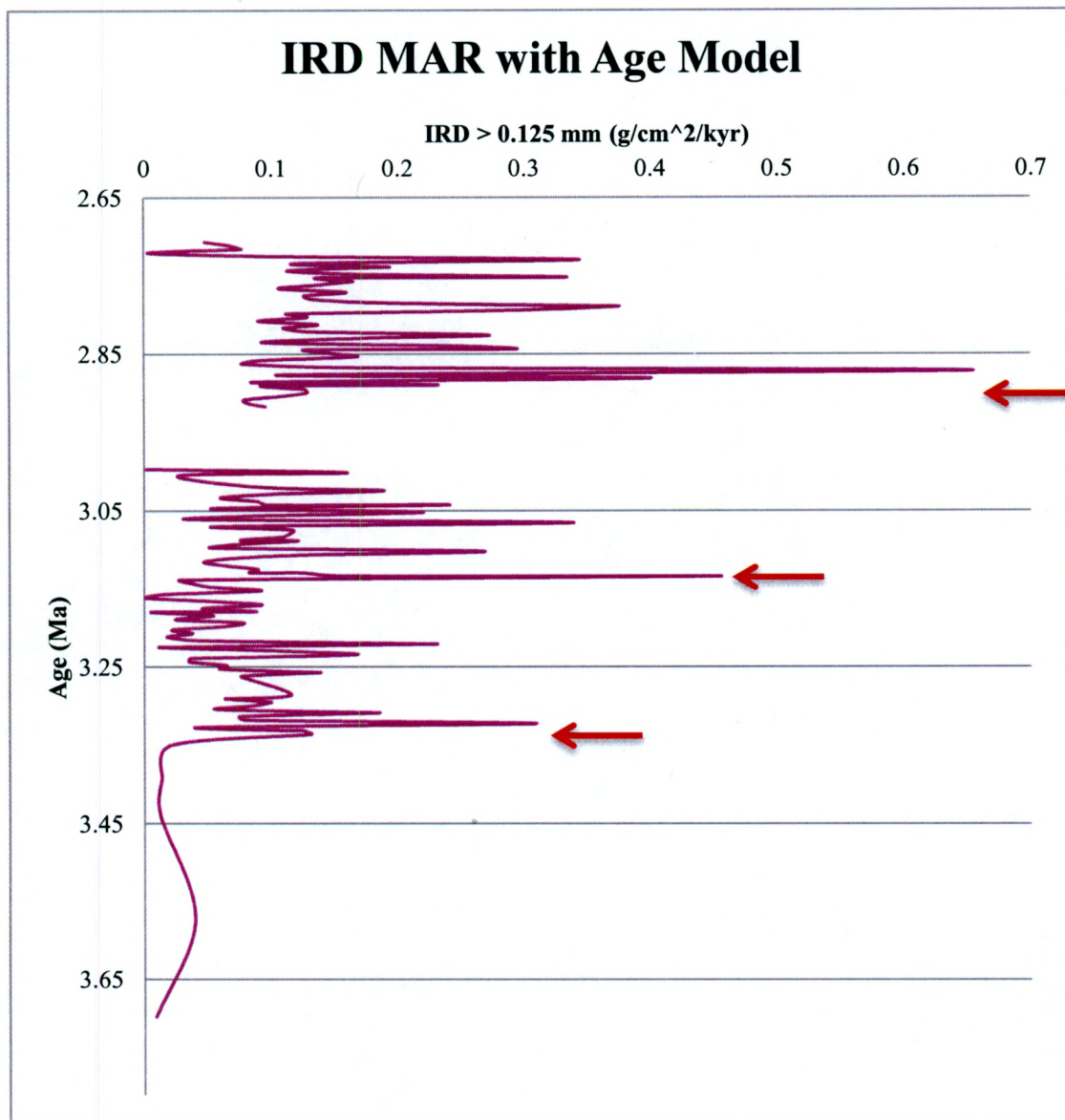
Figure 5. Record of IRD MAR with age model. Red arrows show 3 peaks from which samples were taken to analyze on the SEM.

Figure 6. IRD MAR and Particle Size Distribution in volume percent, adjacent to the lithostratigraphic log for U1359A, with a key for the lithostratigraphic log.

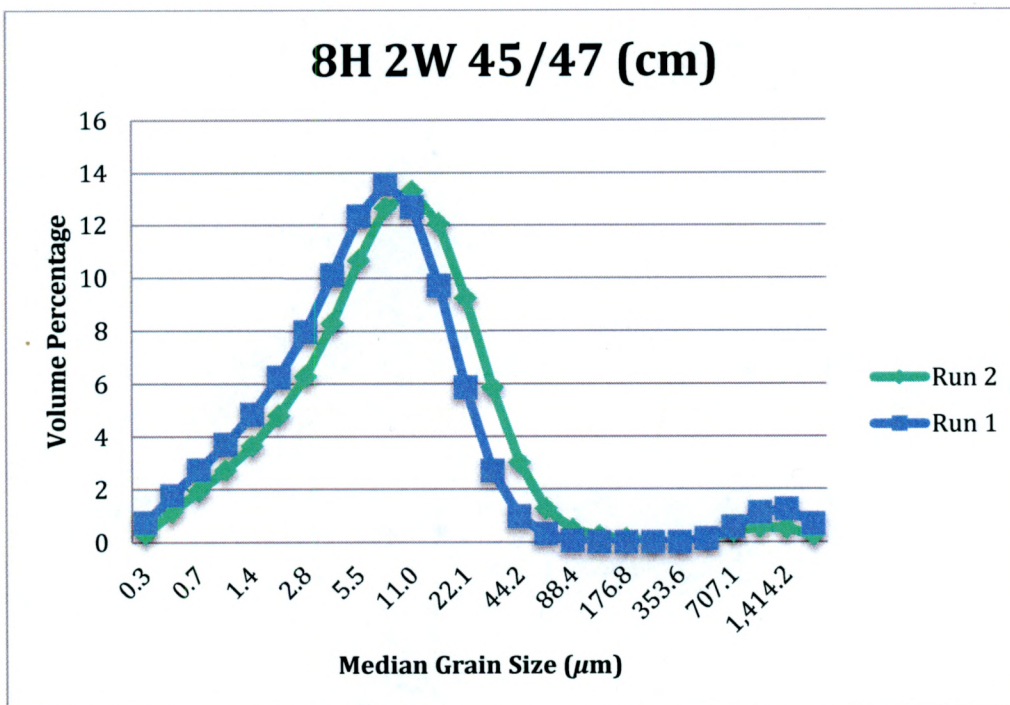**Figure 7.** Grain size distribution comparison of different obscurations.
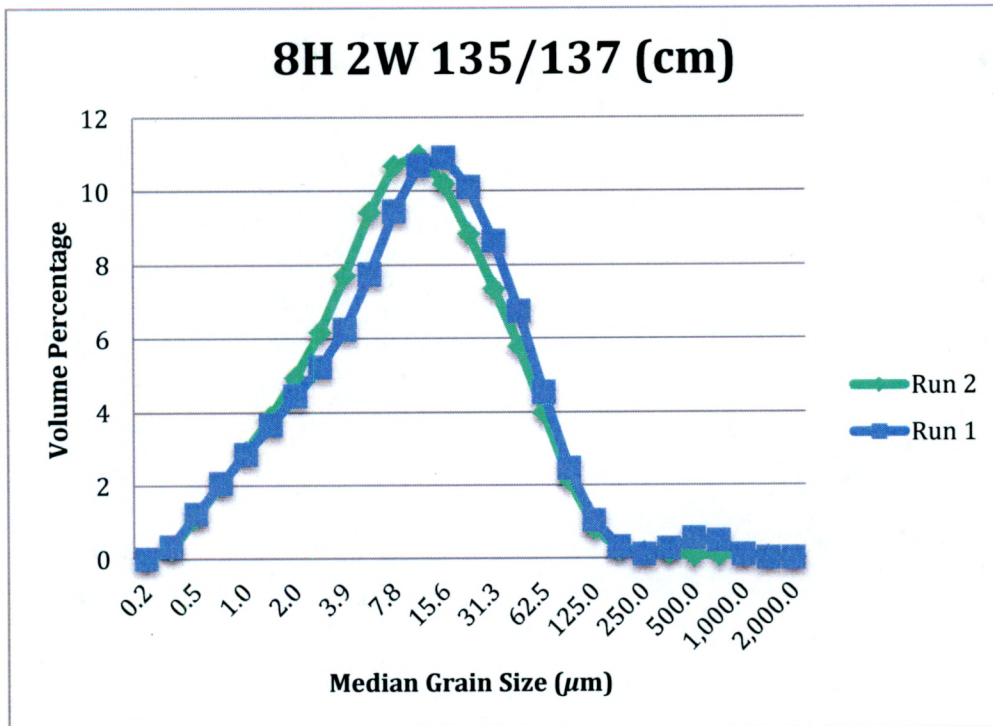Run 1: 43.49%; Run 2: 23.61%.
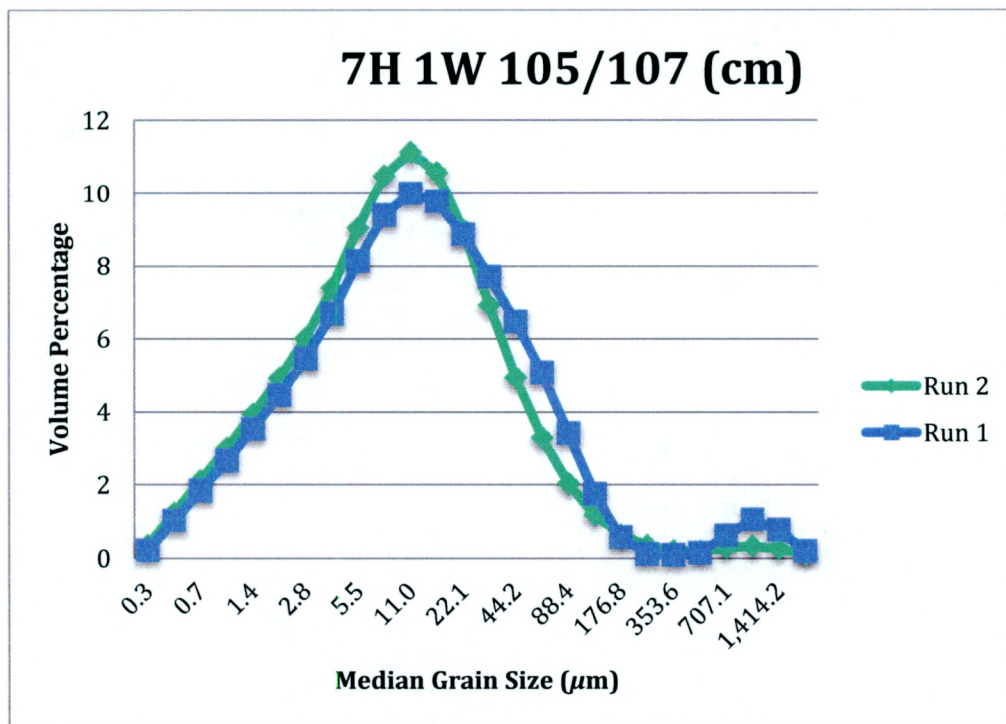
Figure 8. Grain size distribution comparison of different obscurations.
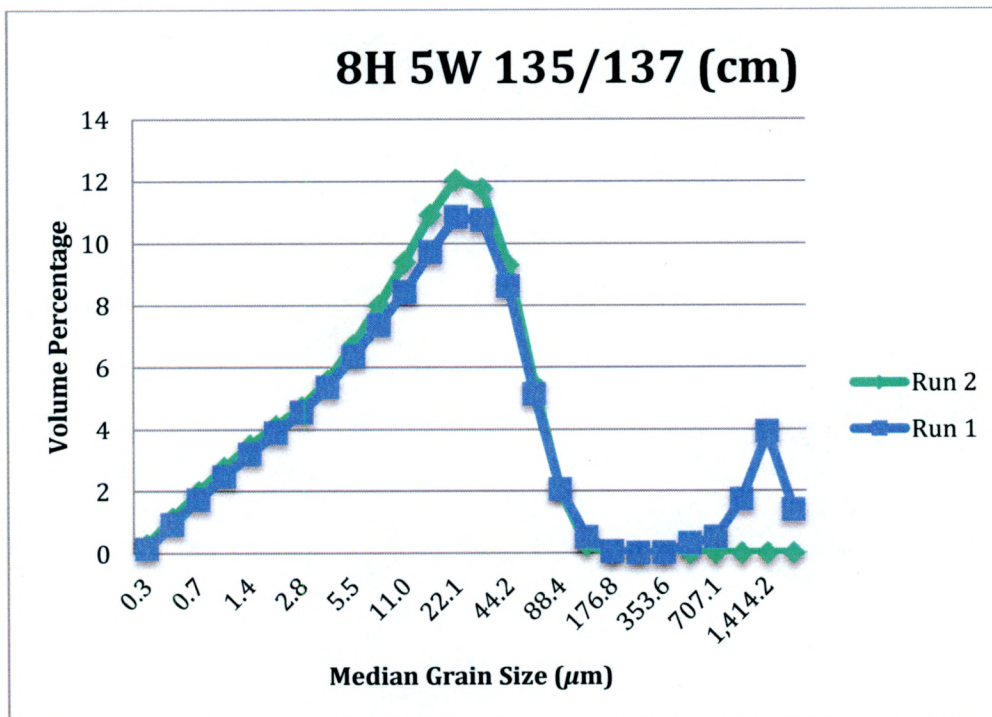Run 1: 5.28%; Run 2: 23.61%.
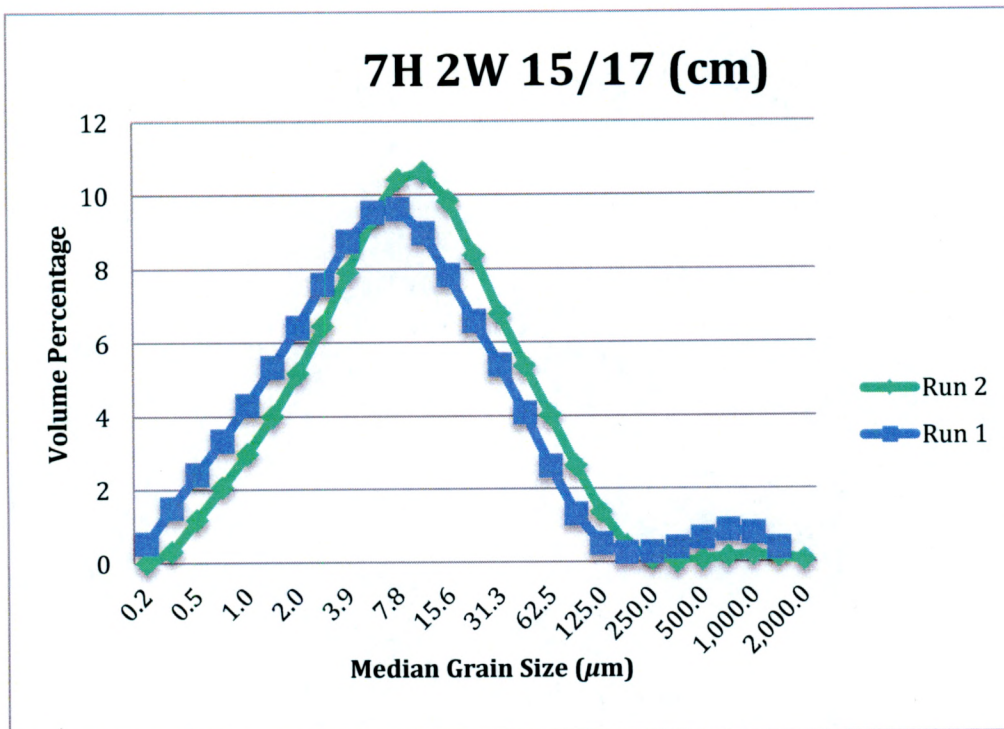
Figure 9. Grain size distribution comparison of different obscurations. Run 1: 40.06%; Run 2: 23.96%.
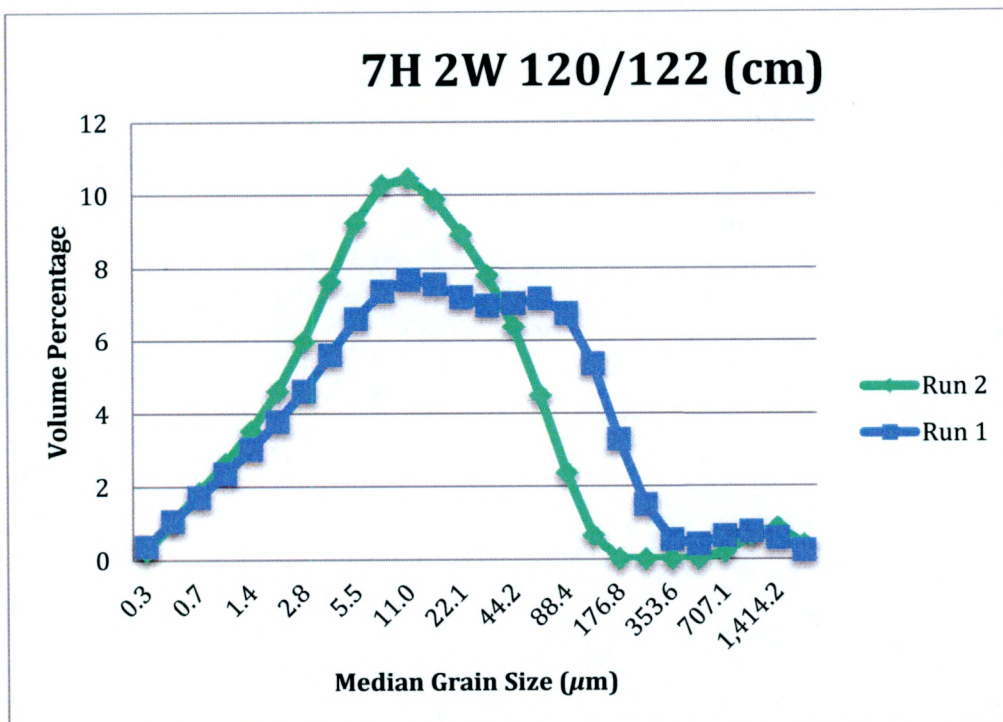
Figure 10: Grain size distribution comparison of different obscurations. Run 1: 43.39%; Run 2: 12.9%.
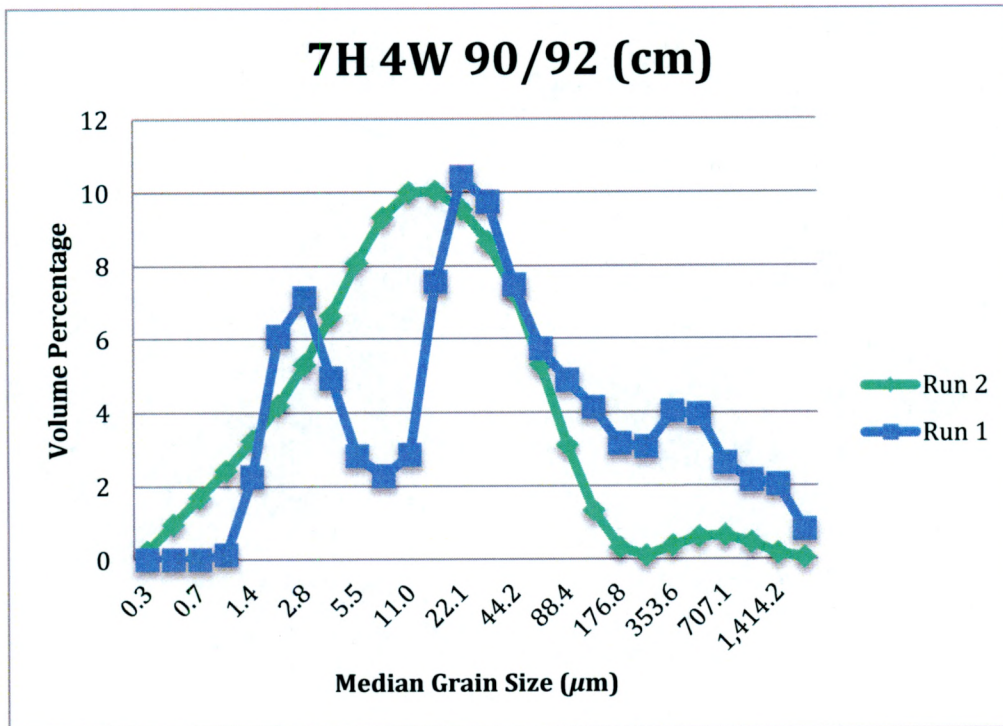
Figure 11: Grain size distribution comparison of different obscurations.
Run 1: 21.26%; Run 2: 10.7%.

Figure 12. Grain size distribution comparison of different obscurations.
Run 1: 43.44%; Run 2: 21.83%.

Figure 13. Grain size distribution comparison of different obscurations. Run 1: 6.25%; Run 2: 10.76%.

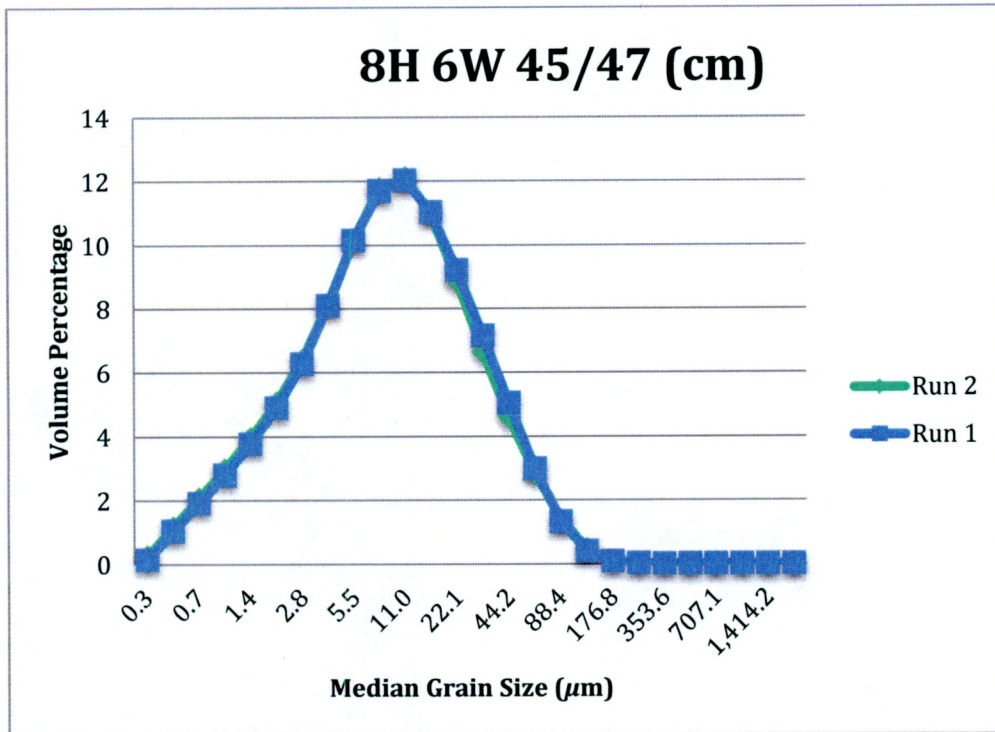**Figure 14.** Grain size distribution comparison of different obscurations. Run 1: 2.77%; Run 2: 14.64%.

Figure 15. Grain size distribution comparison of different obscurations.
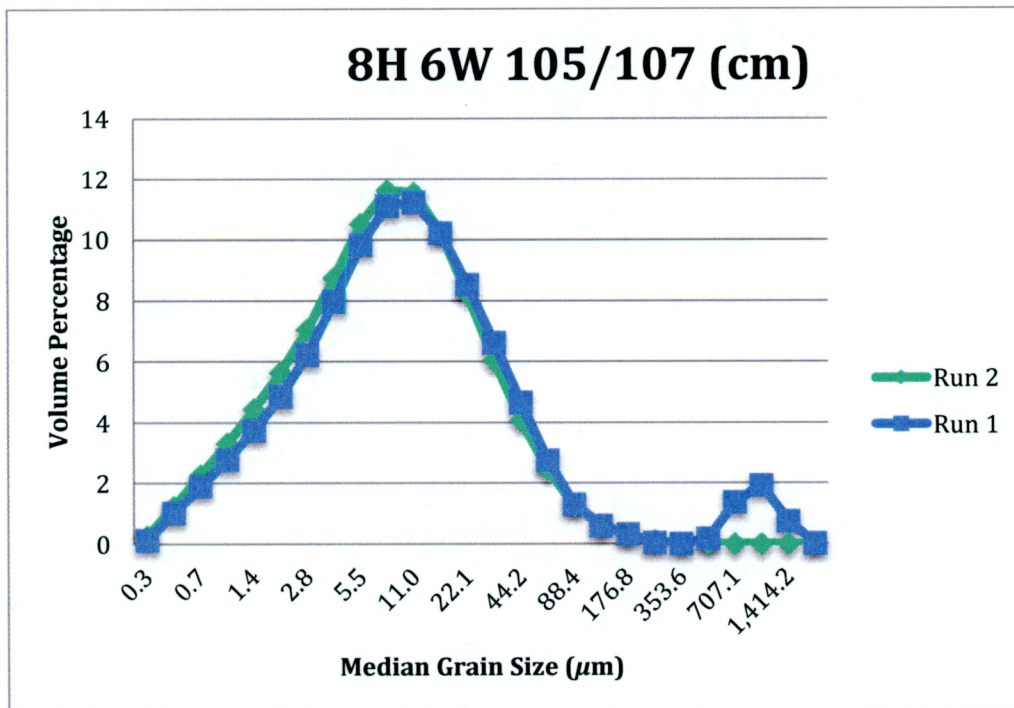Run 1: 6.32%; Run 2: 13.39%.

Figure 16. Grain size distribution comparison of different obscurations.
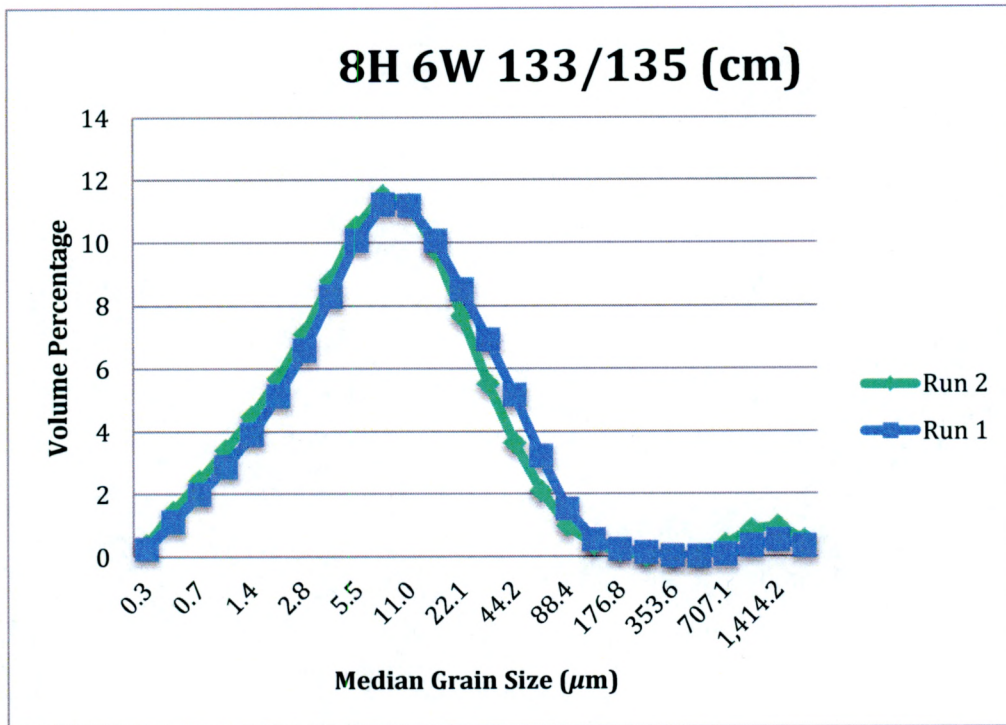Run 1: 5.46%; Run 2: 14.12%.

Figure 17. Grain size distribution comparison of different obscurations.
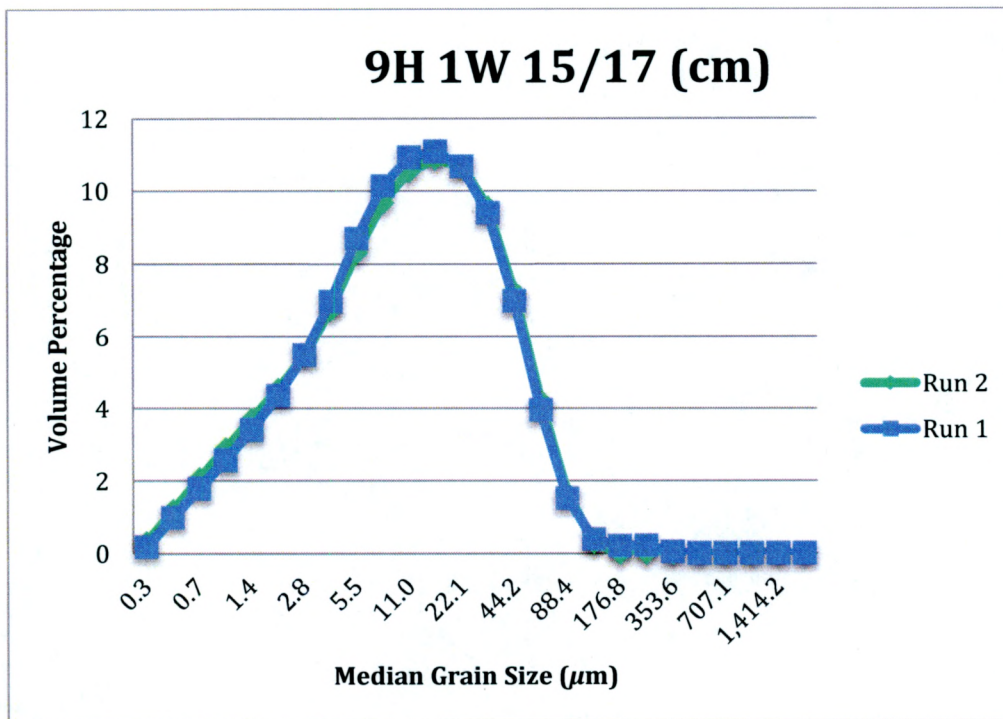Run 1: 5.71%; Run 2: 19.13%.

Figure 18. Grain size distribution comparison of different obscurations.
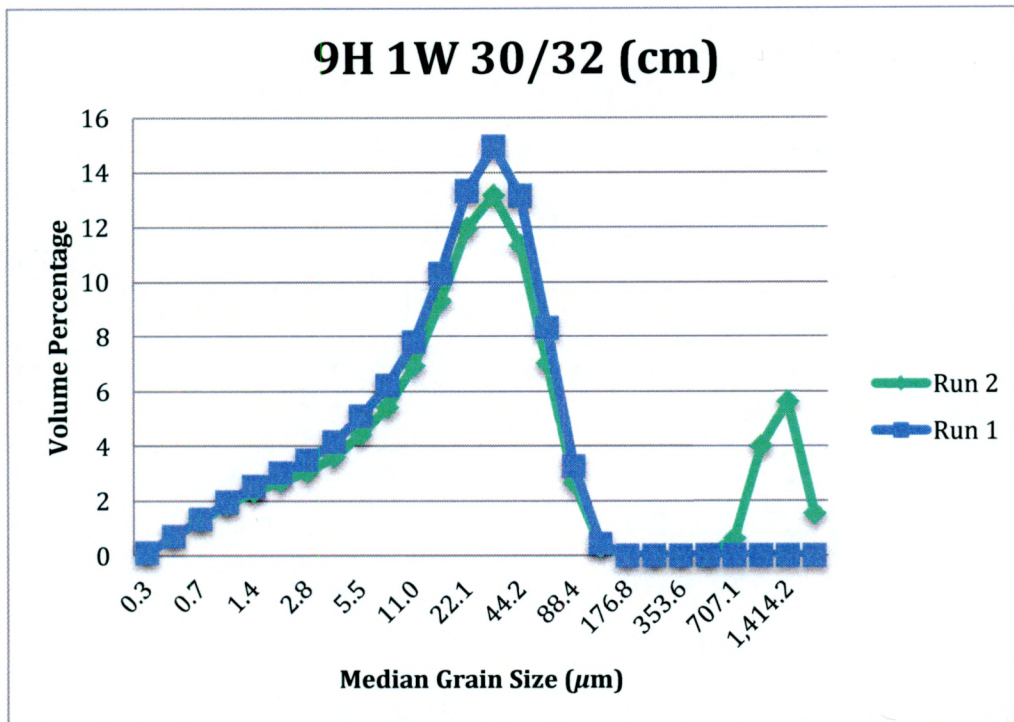Run 1: 4.76%; Run 2: 17.24%.

Figure 19. Grain size distribution comparison of different obscurations.
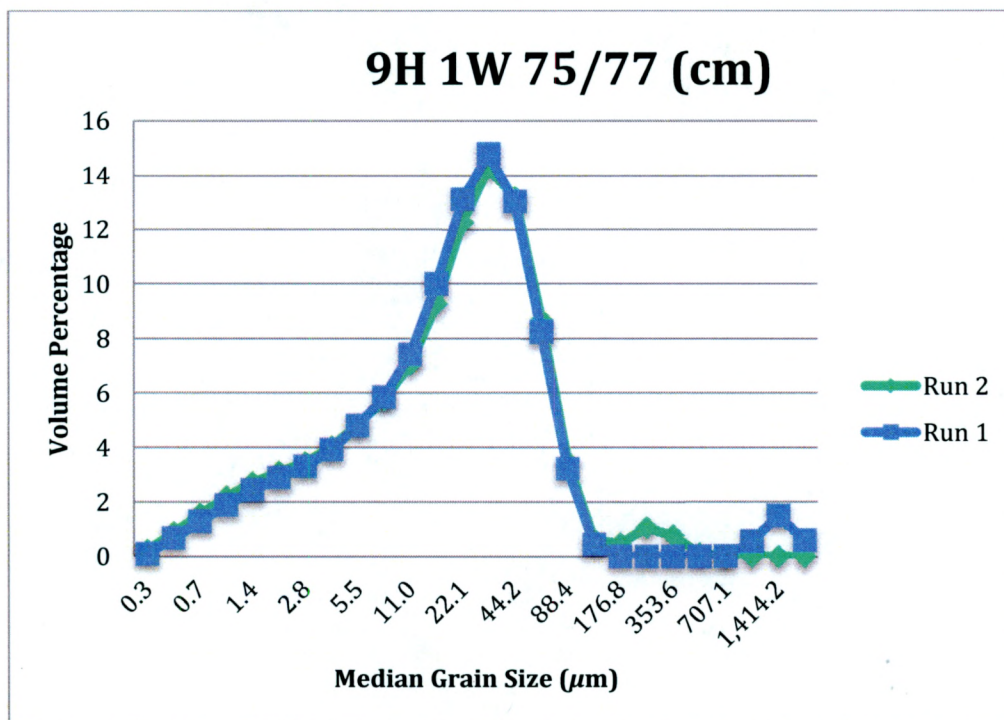Run 1: 5.8%; Run 2: 11.76%.

Figure 20. Grain size distribution comparison of different obscurations.
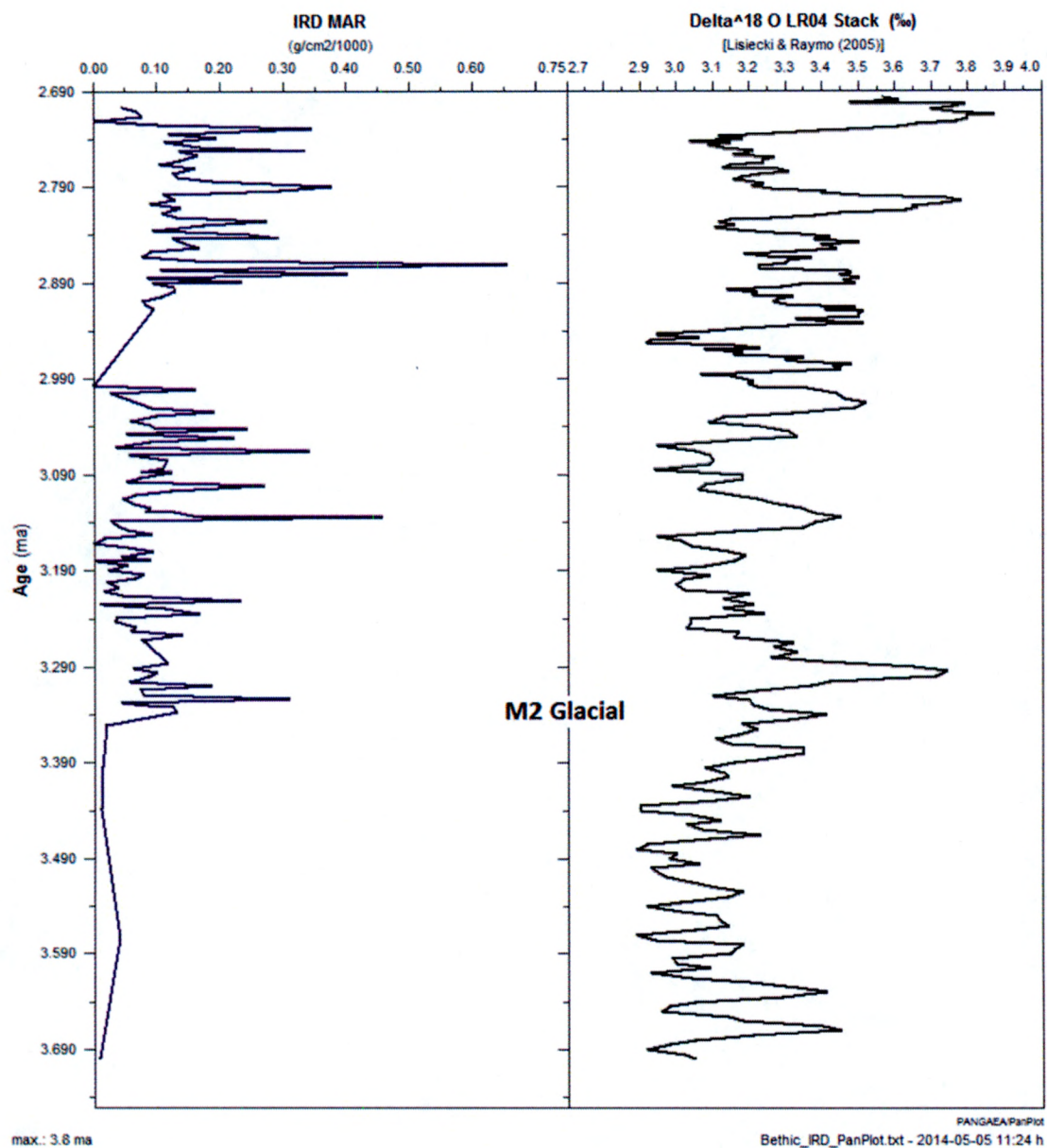Run 1: 1.59%; Run 2: 21.11%.

Figure 21. Record of IRD MAR alongside the $\partial^{18}O$ LR04 stack (per mill) by Lisiecki and Raymo (2005).
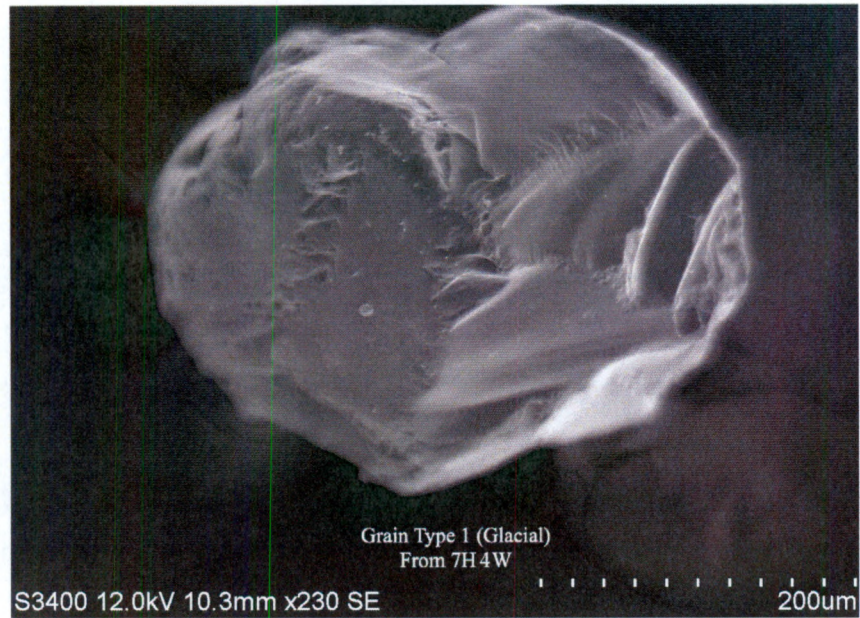
41

Figure 22. Image of Grain Type 1 (Damiani et al., 2006) taken from U1359A section 7H 4W.

Figure 23. Image of Grain Type 2 (Damiani et al., 2006) taken from U1359A section 7H 4W.

Figure 24. Image of Grain Type 3 (Damiani et al., 2006) taken from U1359A section 7H 4W.

Figure 25. Image of Grain Type 2 (Damiani et al., 2006) taken from U1359A section 8H 4W.

Figure 26. Image of Grain Type 3 (Damiani et al., 2006) taken from U1359A section 8H 4W.

Figure 27. Image of Grain Type 1 (Damiani et al., 2006) taken from U1359A section 9H 1W.

Figure 28. Image of Grain Type 2 (Damiani et al., 2006) taken from U1359A section 9H 1W.

Figure 29. Image of Grain Type 3 (Damiani et al., 2006) taken from U1359A section 9H 1W.

Figure 30. Image of Grain Type 4 (Damiani et al., 2006) taken from U1359A section 8H 4W.
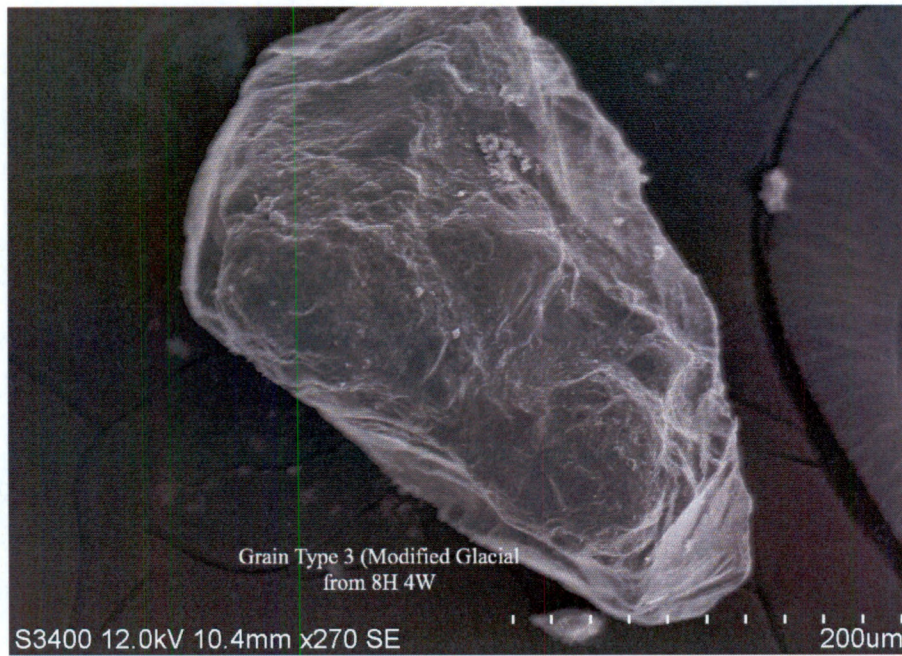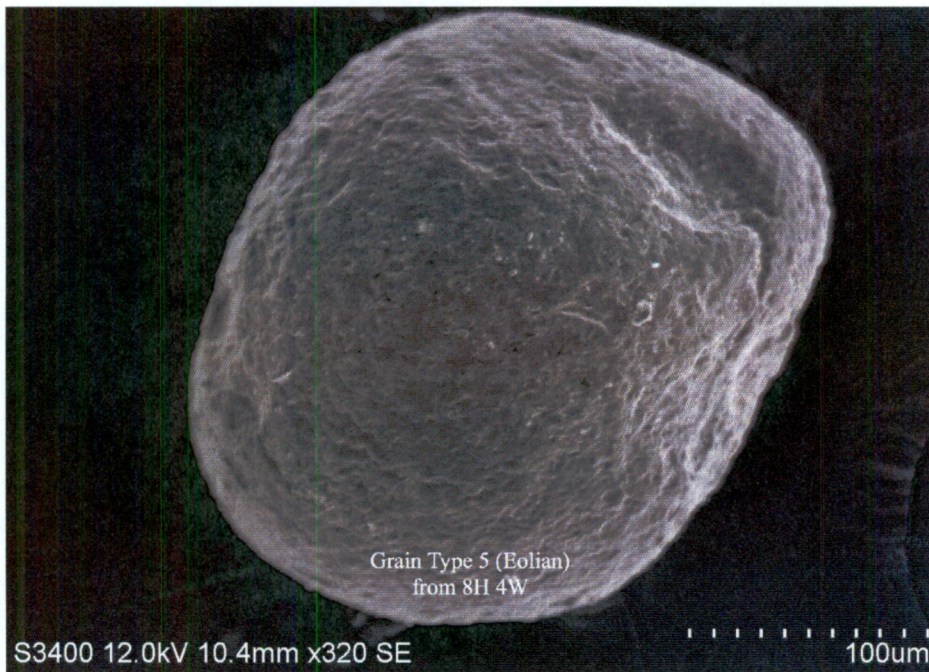

Figure 31. Image of Grain Type 5 (Damiani et al, 2006) taken from U1359A section 8H 4W.
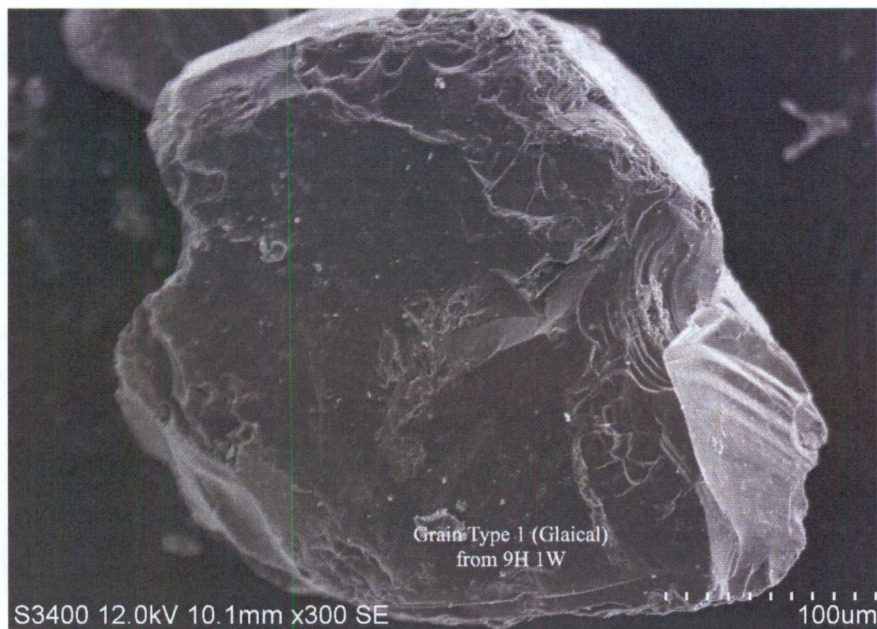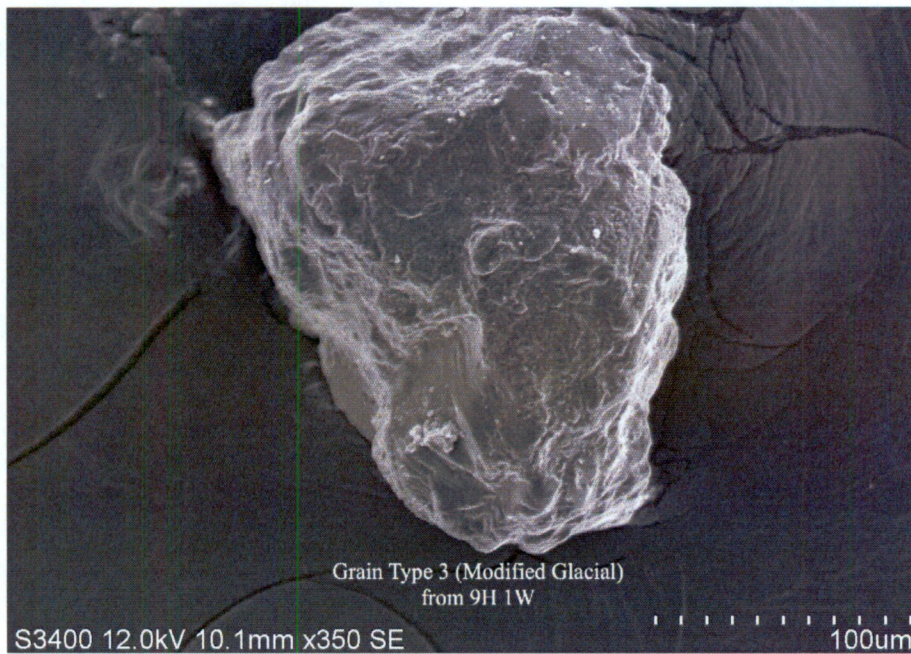
In-image text: Grain Type 6 (Chemically Altered) from 8H 4W
S3400 12.0kV 10.5mm x250 SE   200um
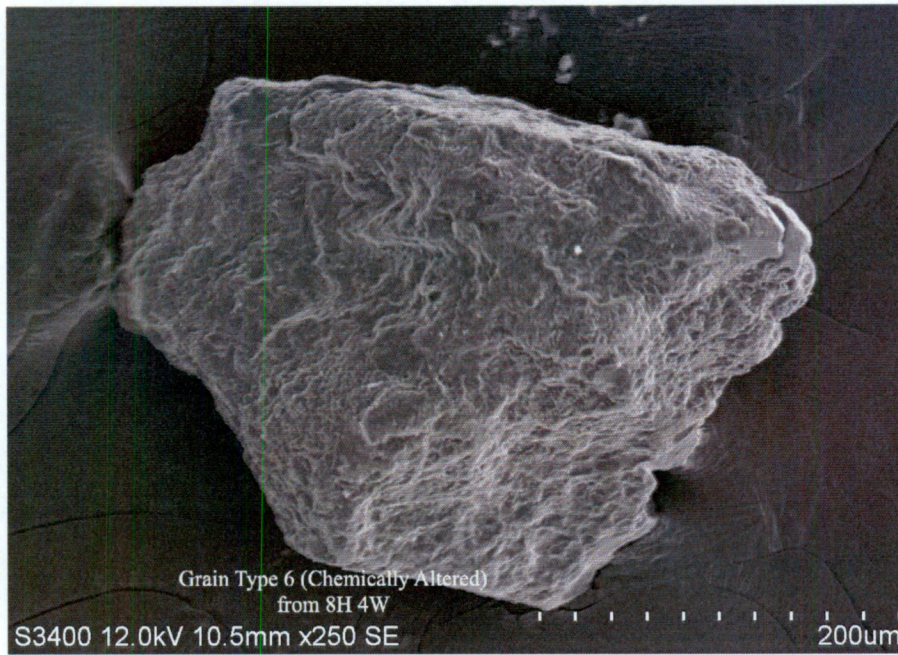
Figure 32. Image of Grain Type 6 (Damiani et al, 2006) taken from U1359A section 8H 4W.
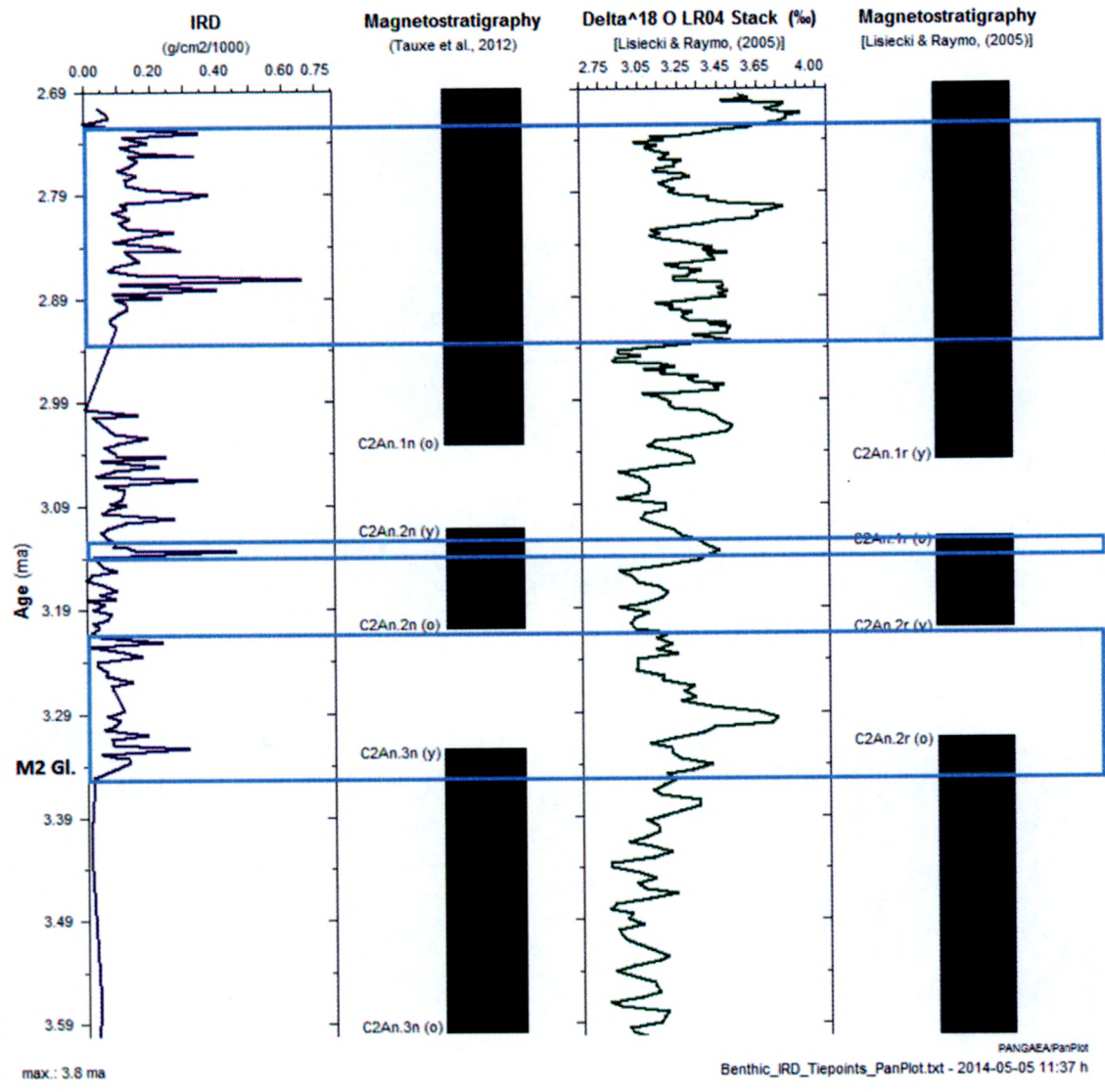
Figure 33. A comparison of IRD MAR and the $\partial^{18}O$ LR04 stack, with magnetostratigraphy for time comparison. Tie points for Tauxe et al. (2012) were used for IRD MAR, and tie points from Lisiecki & Raymo (2005) were used from the benthic record. Blue boxes indicate ice expansion.

IRD MAR
[g/cm2/1000]

CO2 (ppm)
[Seki et al., 2010]

Age [ma]

max.: 3.8 ma

PANGAEA/PanPlot
CO2 Panplot.txt - 2014-05-05 09:34 h
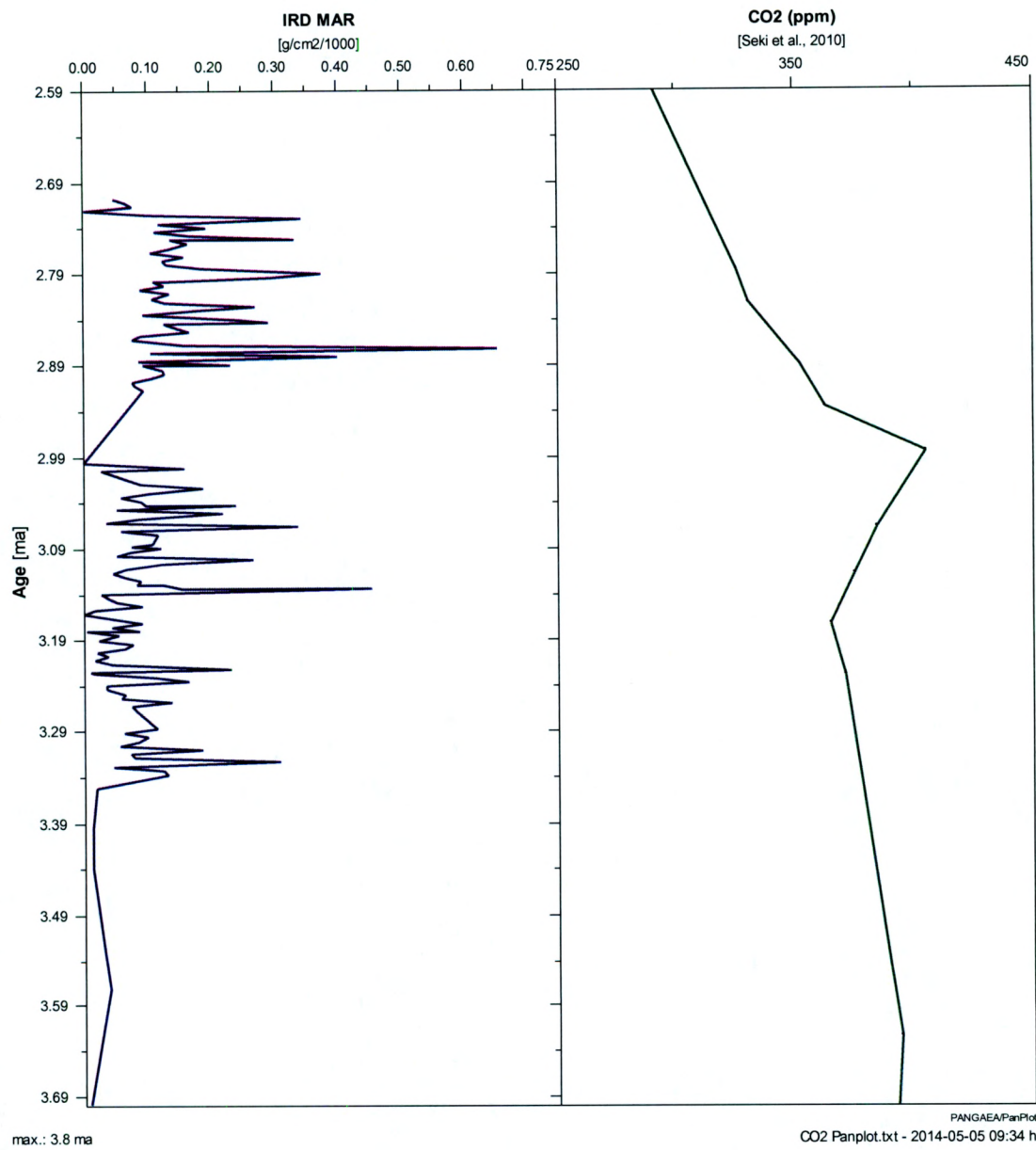
Figure 34. Comparison of IRD MAR from U1359A and CO_2 data (Seki et al., 2010).
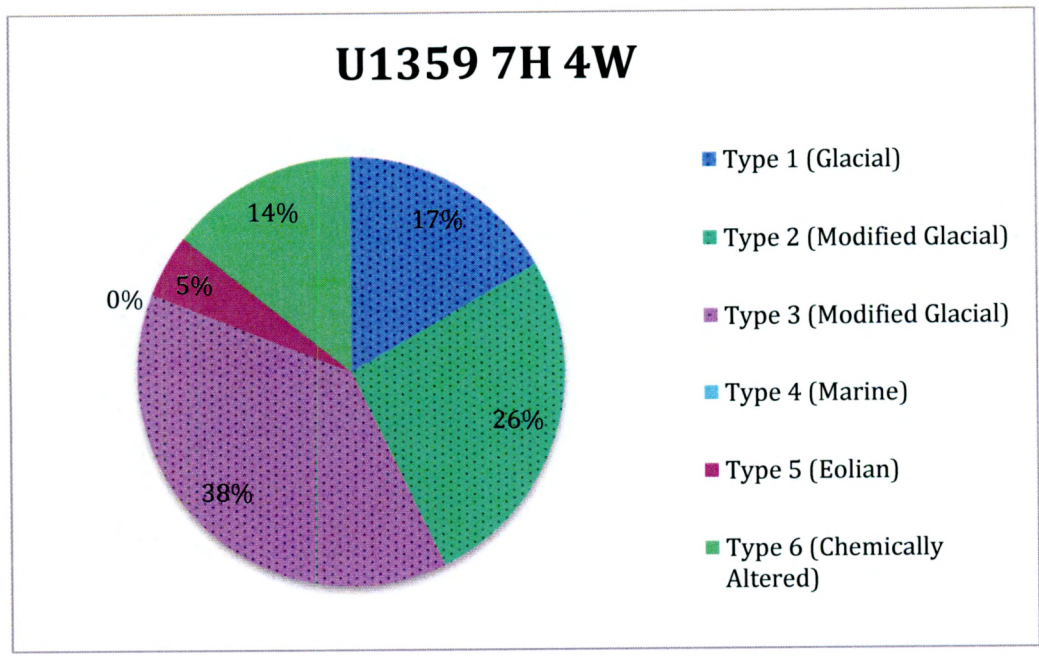
Figure 35. Grain Type percent's for U1359A sample 7H 4W. Stippled texture indicates glacial origin.
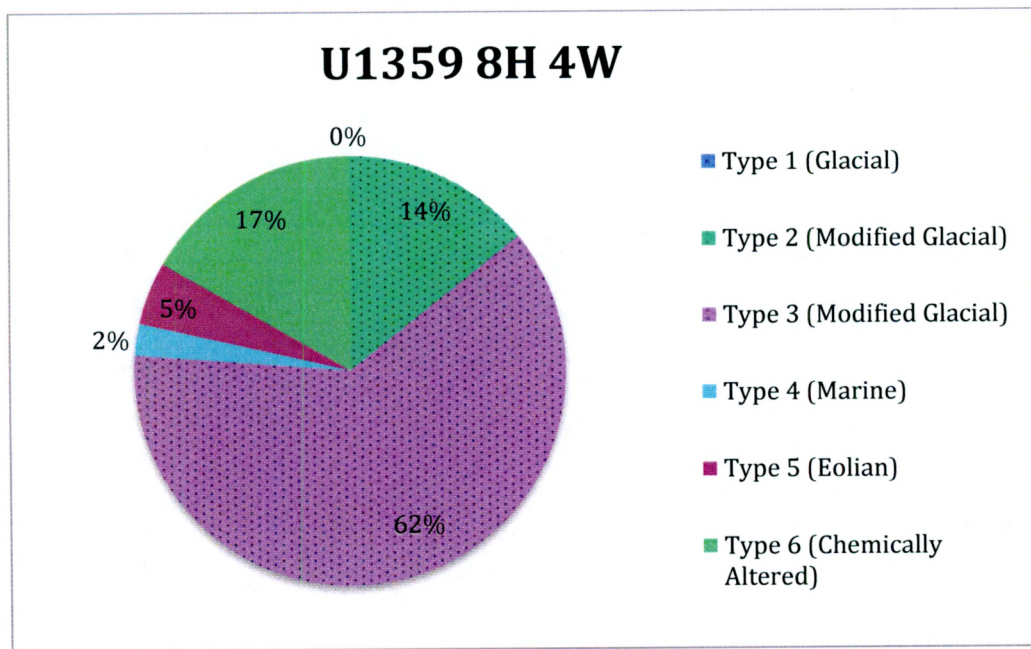
Figure 36. Grain Type percent's for U1359A sample 8H 4W. Stippled texture indicates glacial origin.

U1359 9H 1W

- Type 1 (Glacial)
- Type 2 (Modified Glacial)
- Type 3 (Modified Glacial)
- Type 4 (Marine)
- Type 5 (Eolian)
- Type 6 (Chemically Altered)

0% 0%
0% 8% 7%
36%
49%
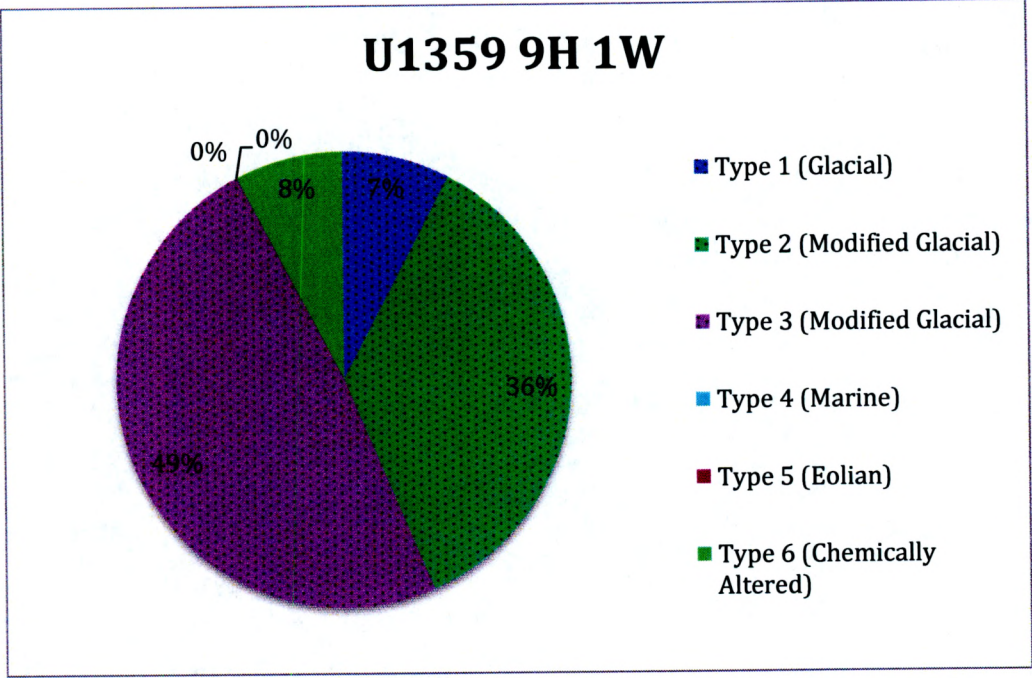
Figure 37. Grain Type percent's for U1359A sample 9H 1W. Stippled texture indicates glacial origin.
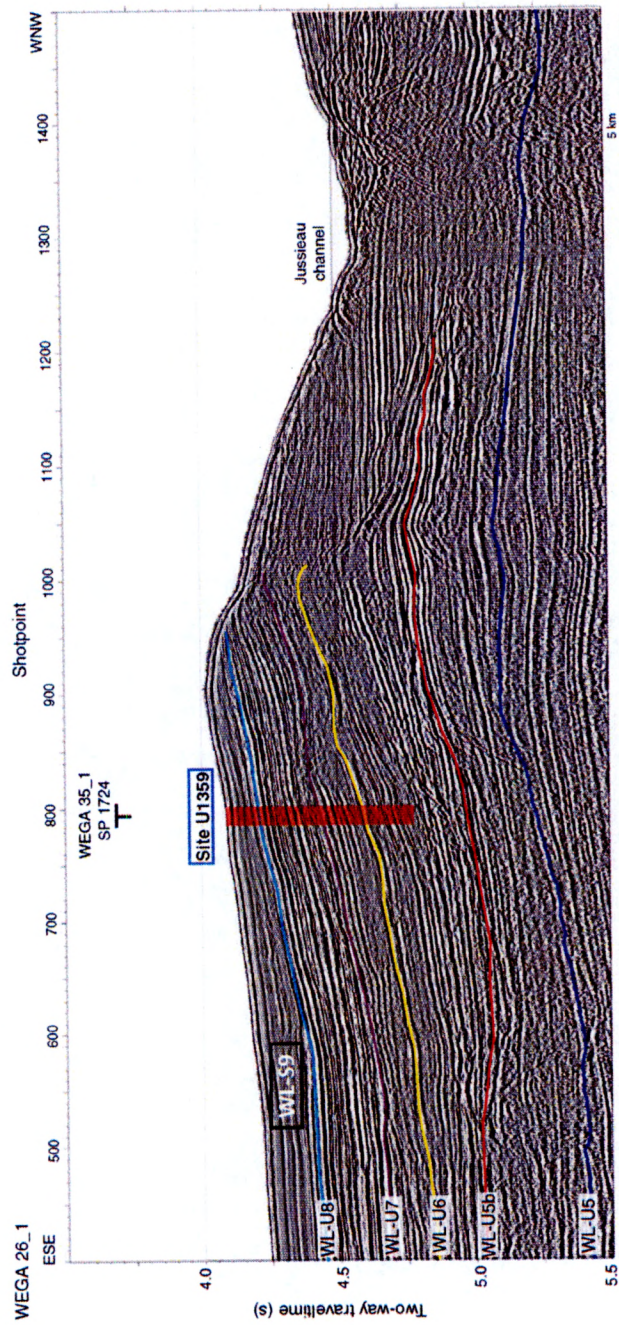
Figure 38. Seismic image of unconformities from Escutia et al. (2011) from U1359 Site Summary IODP Expedition 318. Blue box is site location; black box is WL-S9.
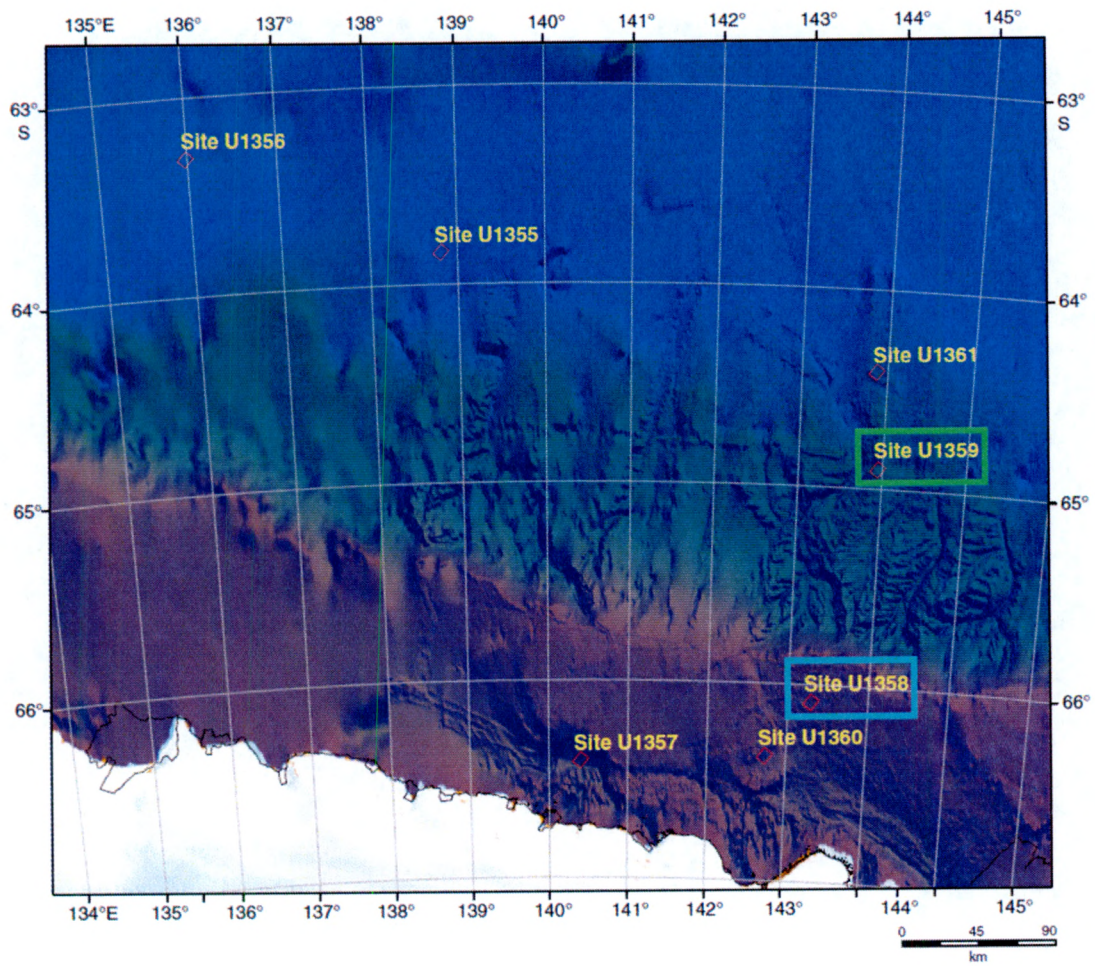
Figure 39. Location of Site U1359, and U1358 (Escutia et al. 2011) from site summary report.
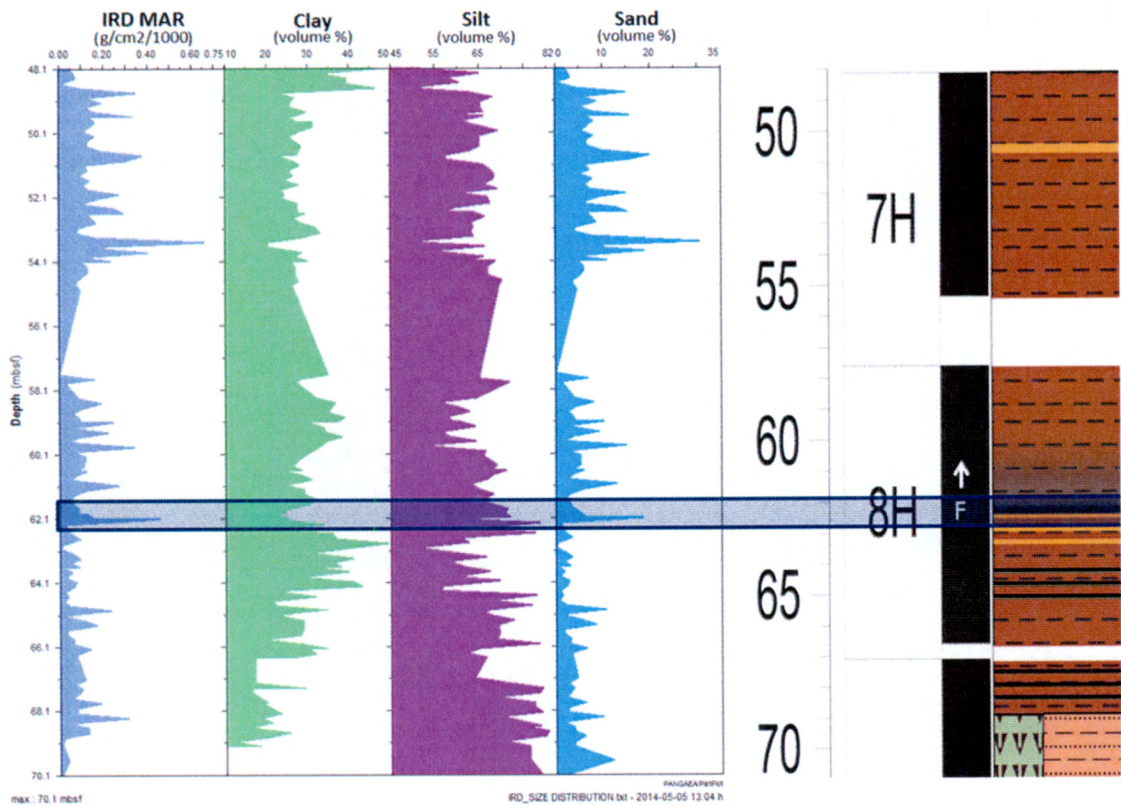
Figure 40. IRD MAR and Particle Size Distribution in volume percent, adjacent to the lithostratigraphic log for U1359A, with a key for the lithostratigraphic log. Blue box indicates that the peak in IRD MAR at ~62.1 mbsf correlates with a fining upward sequence.

Tables

Median Age (Ma)	Top (mbsf)	LSR (m/myr)
2.581	44.05	32.759
3.207	64.1	
3.33	68.85	
3.596	69.75	3.383458647

Table 1. Age Tie-points in millions of years based on U1359A in Tauxe et al. (2012), with linear sedimentation rates.

U1359A 7H 4W	
Grain	Classification (Damiani et al. (2006))
Grain 1	3
Grain 2	3
Grain 3	3
Grain 4	2
Grain 5	6
Grain 6	6
Grain 7	1
Grain 8	3
Grain 9	2
Grain 10	3
Grain 11	2
Grain 12	3
Grain 13	2
Grain 14	3
Grain 15	6
Grain 16	2
Grain 17	2
Grain 18	3
Grain 19	3
Grain 20	3
Grain 21	3
Grain 22	5
Grain 23	3
Grain 24	1
Grain 25	1
Grain 26	1
Grain 27	2
Grain 28	1
Grain 29	1
Grain 30	2
Grain 31	3
Grain 32	5
Grain 33	2
Grain 34	6
Grain 35	2
Grain 36	3
Grain 37	6
Grain 38	2
Grain 39	3
Grain 40	3
Grain 41	1
Grain 42	6

Table 2. Classification of grains in U1359A 7H 4W using Damiani et al. (2006)

U1359A 8H 4W	
Grain	Classification (Damiani et al. (2006))
Grain 1	2
Grain 2	6
Grain 3	6
Grain 4	1
Grain 5	3
Grain 6	3
Grain 7	6
Grain 8	3
Grain 9	3
Grain 10	4
Grain 11	3
Grain 12	3
Grain 13	3
Grain 14	6
Grain 15	2
Grain 16	3
Grain 17	3
Grain 18	3
Grain 19	3
Grain 20	3
Grain 21	3
Grain 22	6
Grain 23	6
Grain 24	3
Grain 25	2
Grain 26	3
Grain 27	3
Grain 28	3
Grain 29	2
Grain 30	3
Grain 31	3
Grain 32	2
Grain 33	3
Grain 34	5
Grain 35	5
Grain 36	3
Grain 37	3
Grain 38	3
Grain 39	3
Grain 40	6
Grain 41	3
Grain 42	2
Grain 43	3

Table 3. Classification of grains in U1359A 8H 4W using Damiani et al. (2006).

U1359A 9H 1W	
Grain	Classification (Damiani et al. (2006))
Grain 1	2
Grain 2	2
Grain 3	3
Grain 4	2
Grain 5	2
Grain 6	3
Grain 7	3
Grain 8	3
Grain 9	1
Grain 10	2
Grain 11	3
Grain 12	2
Grain 13	3
Grain 14	1
Grain 15	2
Grain 16	2
Grain 17	3
Grain 18	3
Grain 19	2
Grain 20	6
Grain 21	3
Grain 22	2
Grain 23	2
Grain 24	3
Grain 25	6
Grain 26	3
Grain 27	3
Grain 28	2
Grain 29	6
Grain 30	2
Grain 31	2
Grain 32	3
Grain 33	3
Grain 34	3
Grain 35	3
Grain 36	3
Grain 37	3
Grain 38	3
Grain 39	1

Table 4. Classification of grains in U1359A 9H 1W using Damiani et al. (2006).

U1359A 7H 4W	
Origin	Number of Grains
Glacial	34
Marine	0
Eolian	2
Diagenetic	6

Table 5. Number of grains of each origin in U1359A 7H 4W.

U1359A 8H 4W	
Origin	Number of Grains
Glacial	33
Marine	1
Eolian	2
Diagenetic	7

Table 6. Number of grains of each origin in U1359A 8H 4W.

U1359A 9H 1W	
Origin	Number of Grains
Glacial	36
Marine	0
Eolian	0
Diagenetic	3

Table 7. Number of grains of each origin in U1359A 9H 1W.